Title
Understanding the vertical structure of potential vorticity in tropical depressions

Journal
Quarterly Journal of the Royal Meteorological Society, 145(722)

ISSN
0035-9009

Authors
Murthy, Varun S
Boos, William R

Publication Date
2019-07-01

DOI
10.1002/qj.3539

Peer reviewed

Understanding the vertical structure of potential vorticity in tropical depressions

Varun S. Murthy[1], William R. Boos[2,3]

[1]Department of Geology and Geophysics, Yale University, New Haven, Connecticut, USA [2]Department of Earth and Planetary Science, University of California, Berkeley, California, USA [3]Climate and Ecosystem Sciences Division, Lawrence Berkeley National Laboratory, Berkeley, California, USA

Correspondence Varun S. Murthy, Department of Geology and Geophysics, Yale University, P.O. Box 208109, New Haven, CT 06520-8109, USA. Email: varun.murthy@yale.edu

Abstract

Potential vorticity (PV) has been used to understand the intensification and motion of a variety of tropical vortices. Here, atmospheric reanalyses and idealized models are used to understand how the vertical structures of moist convective heating and adiabatic advection jointly shape the vertical structures of PV in tropical depressions. Observationally based estimates reveal a top-heavy PV structure in tropical depressions, contrasting with bottom-heavy structures of absolute vorticity and diabatic PV generation. These distinct vertical structures are reproduced in an axisymmetric model which employs the weak temperature gradient approximation for conceptual simplicity and is forced by stratiform and deep convective heating. When applied in isolation, the stratiform and deep convective heatings produce PV maxima at 500 hPa and near the surface, respectively. When these two heatings are applied simultaneously, interactions between the stratiform and deep convective modes enhance the adiabatic advective tendencies produced by the transverse circulation, making the PV distribution more top-heavy. In the lower and middle troposphere, radial advection also greatly reduces the radius of the PV structure relative to that of the imposed heating, consistent with structures in observed tropical depressions; the implications of these differences in radial structures for using the flux form of the relevant conservation equations (e.g. for PV substance or absolute vorticity) are discussed.

KEYWORDS: convective and stratiform clouds, potential vorticity, tropical depressions

1 INTRODUCTION

The examination of potential vorticity (PV) has improved understanding of a wide range of dynamical phenomena in planetary fluids, primarily due to the conservation and invertibility properties of this tracer (e.g. Hoskins *et al.* 1985). Ertel's PV (Rossby, 1940; Ertel, 1942) is conserved in adiabatic, inviscid flow, enabling its treatment as a passive tracer in such motion. Additionally, due to its invertibility, wind and mass fields can be obtained knowing only the scalar PV, given appropriate boundary and balance conditions. Tropical cyclone (TC) circulations exist far from the adiabatic, inviscid limit in which PV is conserved as a Lagrangian tracer, but the study of PV evolution in these storms has nevertheless provided insight on their intensification and motion (Kepert, 2010, and references therein). The purpose of this study is to improve understanding of processes that set the vertical structure of PV during tropical depression (TD) spin-up, an early stage of TC genesis.

Early studies of the evolution of PV in TCs used axisymmetric, isentropic models of varying complexity and found mature TCs to have a deep maximum in PV throughout the troposphere and a minimum at the tropopause (e.g. Thorpe, 1985; Schubert and Alworth, 1987; Möller and Smith, 1994; Delden, 2003; Hausman *et al*. 2006). In these idealized models, latent heating diabatically generates PV at lower levels and destroys it at upper levels, and subsequent vertical advection deepens the low-level PV maximum and reduces the vertical extent of the upper-level minimum. This PV structure of mature TCs was corroborated by observations, which found large values of PV throughout the lower and middle troposphere within the TC eyewall and low values aloft (e.g. Shapiro and Franklin, 1995; Wu and Kurihara, 1996).

Less attention has been given to PV during the earlier stage of TD spin-up, with analyses limited mostly to case-studies. Tory *et al*. (2006) found PV diabatically generated at both lower and middle levels during TC formation, while Yuan and Wang (2014) found mid-level PV maxima. Raymond (2012) argued that the mid-level PV maximum and accompanying warm-over-cold thermal structure aided further intensification. Yu *et al*. (2010) also found that the PV was a maximum at mid-levels during the merger of mesoscale vortices in TD spin-up, with Ritchie and Holland (1997) suggesting that the increase in PV during such mergers increased the vertical depth of the vortex and led to the formation of a low-level vortex. The structure of PV was also examined in monsoon depressions, which are precipitating cyclonic vortices of similar horizontal scale to TDs but which form in monsoonal basic states with large vertical shear. Hurley and Boos (2015) found that monsoon depressions in multiple monsoon regions appeared as mid-level PV maxima in an atmospheric reanalysis, with the peak PV centred near 500 hPa and a secondary maximum near 700–800 hPa. This structure was corroborated by Hunt *et al*. (2016) in the Indian monsoon and by Berry *et al*. (2012) in the Australian monsoon. Additionally, Boos *et al*. (2017) found mid-level filaments of high PV streaming out of a region of stratiform convection in the downshear quadrant of one reanalyzed Indian monsoon depression, and hypothesized that this diabatically generated PV might aid in the northwestward motion of Indian monsoon depressions. Similarities exist in the genesis statistics and dynamical structures of monsoon depressions and nascent TCs (Cohen and Boos, 2016; Ditchek *et al*. 2016), so insight on the evolution of PV in TDs might also apply to monsoon depressions, and vice versa.

Characterizing and understanding the distribution of PV in tropical disturbances is important because PV has been used to understand the motion and intensification of those disturbances. While conservation equations of both absolute vorticity and PV can be used to describe the motion of TCs, the PV budget presents a more compact description, especially in baroclinic environments (Shapiro, 1996; Chan *et al*. 2002; Chan, 2005). Boos *et al*. (2015) used the PV budget of Indian monsoon depressions to explain their observed westward motion against the low-level eastward monsoon flow. Furthermore, the influence of large-scale flows such as upper-level baroclinic troughs on TC intensification has been investigated by examining the interaction between respective PV anomalies (e.g. Bosart and Bartlo, 1991; McIntyre, 1993; Molinari *et al*. 1998). When precipitating vortices are subject to a vertically sheared environment, the diabatic evolution of PV can also be used to understand aspects of their motion and tilting (e.g. Raymond and Jiang, 1990), and their possible amplification through baroclinic processes (e.g. de Vries *et al*. 2010; Cohen and Boos, 2016). To be clear, here we do not examine the specific interactions that control the motion and intensification of TDs, but focus instead on processes that shape the vertical structure of PV during TD spin-up.

Understanding the vertical structure of PV in TDs may be particularly important because of the ubiquity of mid-level vortices in the early stages of TC genesis, as seen in field campaign observations (e.g. Bister and Emanuel, 1997; Raymond *et al*. 1998) and numerical simulations (e.g. Wang, 2012). Raymond and Sessions (2007) found that convective stability of the troposphere, created by the warm-over-cold stratification associated with a mid-level vortex, aids in the creation of bottom-heavy convective mass flux profiles that are efficient in converging absolute vorticity at low levels; this suggests that mid-level vortex formation aids spin-up of the warm-core TC circulation. However, there is disagreement about the role of and processes responsible for the mid-level vortex in TC spin-up, with some recent studies showing that spin-up occurs more rapidly in a simulation where mid-level vortex formation was suppressed by eliminating ice processes (e.g. Lussier *et al*. 2014; Kilroy *et al*. 2018) and other studies reporting the absence of TD formation when the latent heat of fusion due to depositional ice growth is removed (Cecelski and Zhang, 2016).

The evolution of PV and vorticity during TD spin-up is expected to be strongly controlled by the vertical and horizontal structure of diabatic heating (Eliassen, 1951). Indeed, Hack and Schubert (1986) showed that the evolution of the vortex was influenced by the vertical and radial distributions of diabatic heating. Diabatic heating is commonly classified into convective and stratiform profiles in organized convection in general (Houze, 2014) and TDs in particular (Houze, 1989; Fritz *et al*. 2016). Deep convective clouds are characterized by low-level convergence and upper-level divergence, with maximum heating in the mid-troposphere diabatically generating PV in the lower troposphere and destroying it in the upper troposphere. Stratiform clouds are characterized by mid-level convergence and upper- and lower-level divergence. In these stratiform clouds, condensation and freezing heat the upper troposphere while melting and evaporation cool below, with positive PV diabatically generated in the mid-troposphere and destroyed at upper and lower levels (Houze, 1997). Wang *et al*. (2010) showed that convective and stratiform precipitation rates both increase during TC genesis, with the heating profile becoming more convective over time. Zawislak and Zipser (2014b) also showed that convective heating occurs over a larger area and in more organized clusters in developing disturbances than in non-developing disturbances. The importance of deep convective clouds during TD spin-up was further shown by Houze *et al*. (2009), who observed intense deep convective cells of roughly 10 km width. Houze (1982) and Wang (2012) suggested that stratiform clouds in TDs had missing or weak low-level divergence, producing mid-level spin-up without the low-level spin-down associated with typical stratiform profiles.

All of these results raise several questions about the origin of the PV structure of depressions. Is the mid-level PV maximum observed in TDs and monsoon depressions created by diabatic PV generation at mid-levels in stratiform clouds, or by adiabatic advection of diabatic PV generated at low levels in deep convective clouds? If stratiform heating is needed to spin up a mid-tropospheric PV maximum, must that heating occur in isolation without strong deep convective heating and its bottom-heavy PV generation? Early studies of PV in precipitating tropical disturbances focused on the vertical structures of PV generated by diabatic heating; as stated by Tory *et al*. (2012), such treatments “provide little insight into the changing primary circulation and PV structure during and after the fluid adjusts to the PV source or sink.” Indeed, Tory *et al*. (2012) showed that diabatic PV generation is typically strongly opposed by adiabatic advection in deep convecting systems, and recommended the isentropic PV substance (PVS) framework of Haynes and McIntyre (1987) as one alternative perspective, albeit one that requires using isentropic coordinates and working with a substance that is not Ertel's PV. Here we examine how stratiform heating, deep convective heating, and adiabatic flow jointly shape the vertical structure of PV in a selection of observed Atlantic TDs and in idealized models of TDs. This applies more general concepts of PV evolution in convectively coupled disturbances (e.g. Haynes and McIntyre, 1987; Tory *et al*. 2012) to the particular vertical structures of heating and ascent in TDs.

The next section describes the data and methods used in our observational analyses. Section 3 shows the structures of PV, PVS, and absolute vorticity in observed TDs, and briefly discusses the conservation of PV in isobaric coordinates and PVS in isentropic coordinates. Section 4 describes the time tendencies of PV in observed TDs, then Section 5 uses idealized models to better understand the vertical structure of these tendencies. We end with a short summary and discussion.

2 DATA AND METHODS

2.1 Atmospheric state estimates

Our observational analyses are based on storm-centred composites of Northern Hemisphere TDs compiled using the European Centre for Medium-Range Weather Forecasts Year of Tropical Convection (ECMWF-YOTC, henceforth YOTC) reanalysis (Moncrieff *et al*. 2012). This reanalysis, which includes Northern Hemisphere hurricane seasons only during 2008 and 2009, was chosen because it provides parametrization tendencies that can be used to compute diabatic PV sources. The reanalysis uses a spectral T799 model with 97 vertical levels and we use gridded, pressure-level data at 0.25° × 0.25° horizontal resolution and 6 hr temporal resolution. Isentropic variables are computed by interpolating isobaric data onto isentropic surfaces with vertical resolution of 3 K between 297 and 370 K. Prior to calculating horizontal gradients (e.g. while computing horizontal advection), variables are smoothed using a 5 × 5 point spatial filter to remove grid-scale noise.

The YOTC reanalysis includes temperature tendencies associated with parametrized radiation, turbulent diffusion, cloud microphysics, shallow convection, and deep convection (Dee *et al*. 2011). The cloud microphysics scheme provides temperature tendencies due to latent heating in grid-scale vertical motion, which at T799 resolution will include some stratiform clouds. However, the cloud microphysics scheme could also potentially include latent heating in some convective clouds that have a horizontal extent greater than the grid scale (e.g. Houze *et al*. 2009). While infrequent in the TDs used in this study, the microphysics scheme sporadically includes grid-scale regions of strong heating in the lower troposphere. Thus, heating due to parametrized cloud microphysics in the YOTC reanalysis is not termed as stratiform heating in this study. However, it is later shown that, in the composite mean, this parametrized microphysical heating strongly resembles canonical vertical profiles of heating in stratiform clouds. Furthermore, in the vicinity of TDs below 950 hPa, positive temperature tendencies due to turbulent diffusion, roughly 5 K/day, coincide with negative temperature tendencies of roughly the same magnitude associated with deep convection. Thus, we sum the temperature tendencies from deep convection and turbulent diffusion and collectively term these “deep convection.”

Atmospheric reanalyses have limitations in their representation of the intensity, structure, and position of TCs (Schenkel and Hart, 2012). Due to the coarse spatial resolution of reanalyses, TCs in reanalyses are often of lower intensity than in reality. The time evolution of disturbances in reanalyses is influenced by episodic data assimilation tendencies; at the same time, a lack of *insitu* observations may prevent the realistic representation of TCs. While the YOTC reanalysis employs a spatial resolution finer than most reanalyses and incorporates vastly improved satellite observations, *insitu* observations, and data assimilation techniques (Moncrieff *et al*. 2012), the fidelity of its representation of TCs has not yet been ascertained. However, our focus on the system-scale, composite-mean structure of weak-intensity TCs may make some of the aforementioned issues less problematic than they would be for the study of fine-scale structure of hurricane-intensity vortices.

2.2 Tropical depression tracks

TD tracks are obtained from the International Best Track Archive for Climate Stewardship (IBTrACS; Knapp *et al*. 2010). We use only tracks and intensities reported by Regional Specialized Meteorological Centers (RSMCs) belonging to the World Meteorological Organization (WMO), and discard subtropical and extratropical storms and those that have split and merged. To isolate tracks corresponding to the TD stage, we consider time steps only when the maximum sustained wind is less than 17 m/s, the upper threshold for TDs defined by the National Oceanic and Atmospheric Administration's National Hurricane Center (NOAA-NHC).

We computed storm-centred composites for TDs in the North Atlantic and the West and East Pacific basins, but we present only the North Atlantic composites here due to their qualitative similarities. Our North Atlantic set included 24 TDs, with 14 in 2008 and 10 in 2009. Storm-centred composites were computed by averaging variables relative to the latitude and longitude of the storm centre, with 6-hourly fields first averaged for each TD and subsequently averaged over all members.

TC genesis has been noted to occur at different spatial scales, with evolution of a mid-level vortex occurring at the meso-α (100–1,000 km) scale and formation of a low-level, proto-vortex at the meso-β (10–100 km) scale (Wang, 2012). However, since the formation of the low-level vortex is noticed only in high-resolution numerical simulations (e.g. Nolan, 2007; Wang, 2012) and not commonly in reanalyses, we focus on the evolution of the storm-scale (meso-α) vortex. Thus, in meridional cross-sections, we zonally averaged across 5° longitude relative to the storm centre. Similarly, vertical profiles were obtained by horizontally averaging in a 5° × 5° box around the storm centre.

Finally, due to inconsistencies in the position of the TC centre in IBTrACS and some reanalyses (Schenkel and Hart, 2012), composites were also computed using the location of surface pressure minimum in the YOTC reanalysis as the centre. These composites were roughly similar to the composites computed using IBTrACS, so we present storm-centred composites based on IBTrACS locations.

2.3 Satellite-derived convective and stratiform heating

Diabatic temperature tendencies in the YOTC parametrization schemes are not directly constrained by *insitu* or satellite observations, even though the YOTC reanalysis assimilates such observations to constrain dynamic and thermodynamic variables. So we compare YOTC diabatic temperature tendencies with latent heating rates derived from the precipitation radar on the Tropical Rainfall Measuring Mission (TRMM) satellite. We use the TRMM

3G25 product, which provides 0.5° × 0.5° gridded swaths of latent heating at 19 vertical levels using the Spectral Latent Heating algorithm (SLH; Shige *et al*., 2004, 2007, 2009).

We only use TRMM swaths that cover at least 50% of the 5° × 5° box surrounding the storm centre, within 6 hr of the best-track time. Under this criterion, TRMM-derived latent heating can be compared with YOTC diabatic heating in nine of the 24 North Atlantic TDs. Since our goal is not to perform an exhaustive examination of TRMM-derived latent heating in TDs, we do not examine other products such as the Convective-Stratiform Heating product (CSH; Tao *et al*. 2006).

3 RESULTS I: OBSERVED VERTICAL STRUCTURES

We begin by describing the structure of TDs in the YOTC reanalysis. In the composite mean, an intensifying TD has cyclonic winds across a radius roughly equal to 10° latitude (shading in Figure 1a). The cyclonic winds peak at 700 hPa and at a radius roughly equal to 2° latitude, consistent with previous observations of TDs as mid-level vortices (e.g. Raymond *et al*. 1998; Wang, 2012). The tangential winds are in thermal wind balance with a warm-over-cold stratification, with positive and negative temperature anomalies both near 1 K magnitude (not shown). The secondary radial circulation consists of inward flow in the lower and middle troposphere and outward flow in the upper troposphere (contours in Figure 1a). This secondary circulation has been shown to converge absolute vorticity and result in TC intensification (Emanuel, 2003; Montgomery and Smith, 2017). The composite mean relative humidity is about 30% larger near the TD centre than in the periphery (shading in Figure 1b). Although a cold core exists in the lower troposphere, these higher humidities are associated with enhanced equivalent potential temperature, θ_e, near the TD centre (contours in Figure 1b), consistent with Smith and Montgomery (2012) and Zawislak and Zipser (2014a).

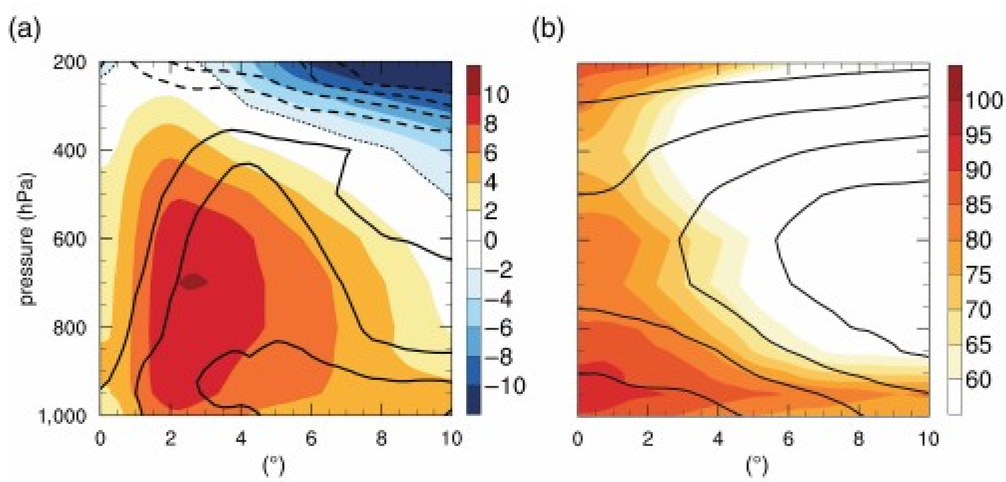

Figure 1. Azimuthally averaged features of the composite mean TD in YOTC reanalysis, with the *x*-axis denoting radial distance from the TD centre in degrees. (a) Tangential wind speed (m/s, colour

shading) and radial wind speed (contours with interval 1 m/s). Negative values of the tangential wind are enclosed with a thin dotted line. (b) Relative humidity (%, colour shading) and equivalent potential temperature θ_e (contours with interval of 5 K, with the radially outermost contour depicting 330 K)

3.1 PV in pressure coordinates

We now examine pressure-coordinate vertical structures of Ertel's PV,

$$q = \frac{1}{\rho}\boldsymbol{\eta} \cdot \nabla\theta, \quad (1)$$

where η is the three-dimensional absolute vorticity vector, θ is potential temperature, and ρ is density. Figure 2a (shading) shows the composite mean PV computed on isobars using the three-dimensional absolute vorticity and θ gradient. The PV exhibits a maximum of magnitude 1.1 PVU (PV units; 1 PVU = 10^{-6}Km^{2}kg^{-1}s^{-1}) in the mid-tropopshere, near 550 hPa, and a secondary maximum of 0.6 PVU in the lower troposphere, near 800 hPa, at the same level as the maximum relative vorticity (contours in Figure 2a). This vertical structure of TDs is distinctly different from the deep column of PV found in early numerical modelling studies of mature TCs, which typically examined the response to a deep convective heating profile (e.g. Schubert and Alworth, 1987). Some observational studies also found that PV in mature TCs has roughly constant amplitude between the surface and upper troposphere (e.g. Shapiro and Franklin, 1995; Molinari *et al*. 1998). However, more recent studies based on high-resolution numerical simulations and field campaigns disagree about the vertical PV structure of mature TCs. Yau *et al*. (2004) found that the PV of a mature TC was bottom-heavy, with maximum values below 3 km altitude. Bell and Montgomery (2008) generally corroborated a bottom-heavy PV structure using field campaign observations of a mature TC, although with a bimodal structure with peaks at 1 and 3 km altitude. In contrast, the numerical simulations of Hausman *et al*. (2006) produced mature TCs with bottom-heavy PV only when latent heating due to ice was switched off, with a mid-tropospheric PV maximum occurring when this effect was included. Mature TCs were also found to have a mid-tropospheric maximum in the numerical simulations of Wang (2008) and Rogers (2010). There is thus no clear agreement about the vertical structure of PV in mature TCs. The bimodal PV structure in North Atlantic TDs documented here, with a stronger mid-tropospheric maximum, closely resembles the PV structure of monsoon depressions (Hurley and Boos, 2015; Hunt *et al*. 2016).

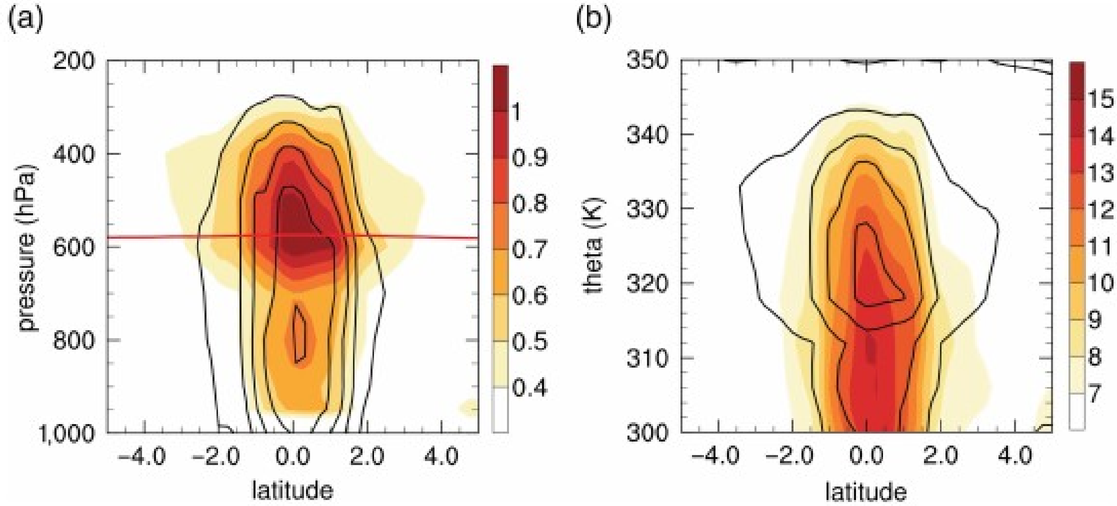

Figure 2. (a) Latitude–height cross-section of the storm-centred composite mean of 2008 and 2009 North Atlantic TDs in ECMWF-YOTC, with shading showing Ertel's PV in PV units and contours showing relative vorticity with contour interval of $2.5 \times 10^{-5} s^{-1}$. The nearly horizontal line at roughly 600 hPa indicates the 0°C melting level. (b) Latitude–potential temperature cross-section of the storm-centred composite mean PV substance (PVS; $10^{-5} s^{-1}$, colour shading,) and PV regridded onto potential temperature surfaces (contours with interval 0.2 PVU with the outermost contour representing 0.4 PVU). All variables are zonally averaged in a 5° longitude band around the storm centre

Relative vorticity peaks in the lower troposphere, near 800 hPa (contours in Figure 2a), consistent with previous studies (e.g. Wang, 2012). Since PV is approximately equal to the product of the vertical component of absolute vorticity and the vertical gradient of potential temperature (Section 5), the comparatively top-heavy PV is due, diagnostically, to an enhanced mid-tropospheric static stability. Note that the warm-over-cold core structure associated with an elevated vortex would have static stability enhanced at the level of peak horizontal wind, which for our composite would produce enhanced static stability and PV at 800 hPa. Some feature other than the anomalous temperature structure of TDs must thus be responsible for the 500 hPa PV maximum; this is further discussed in Section 5.

The mid-tropospheric PV maximum straddles the melting level (the 0°C isotherm; nearly horizontal line at roughly 600 hPa in Figure 2a). This raises the possibility of this mid-level PV maximum being diabatically generated by a canonical stratiform heating profile, which is typically associated with heating above the melting level and cooling below (Houze, 1997). However, the deep convective profile of heating would be expected to generate PV in the lower troposphere, and this deep convective heating is widely thought to dominate nearly all stages of the TC life-cycle, including the TD stage (e.g. Emanuel, 2003; Montgomery and Smith, 2017). Additionally, typical stratiform profiles are associated with divergence in the lower troposphere, potentially leading to the spin-down of a nascent TD. If the observed PV is indeed diabatically generated by a canonical stratiform profile, what prevents negative relative vorticity from appearing at lower levels in Figure 2a? Are the stratiform clouds in TDs atypical, with missing or weak low-level divergence (Houze, 1982; Wang, 2012), or does a combination of deep convective and stratiform heating generate the distinct vertical structures of PV and relative vorticity? These questions are explored below.

3.2 PVS in isentropic coordinates

Many of the seminal studies that used PV to understand atmospheric dynamics employed isentropic coordinates because of the ability of that coordinate system to illustrate Lagrangian motion in approximately adiabatic flow (e.g. Hoskins *et al*. 1985). Furthermore, Haynes and McIntyre, 1987 (1987, 1990) showed that PVS, the product of PV and isentropic density, is globally conserved between isentropes, even in the presence of diabatic heating and friction. Denoted as η_θ, PVS in isentropic coordinates takes the simple form of the vertical component of absolute vorticity, that is, $\eta_\theta = \partial_x v_\theta - \partial_y u_\theta + f$, where (u_θ, v_θ) is the horizontal isentropic velocity and f is the Coriolis parameter. The flux form of the PVS conservation equation is

$$\frac{\partial \eta_\theta}{\partial t} = -\nabla \cdot \left[(u_\theta, v_\theta, 0)\, \eta_\theta + \dot{\theta} \left(\frac{\partial v_\theta}{\partial \theta}, -\frac{\partial u_\theta}{\partial \theta}, 0 \right) \right], \quad (2)$$

where $\dot{\theta}$ is the diabatic heating rate. If this equation is horizontally integrated over a heated region bounded by $\dot{\theta} = 0$ and the divergence theorem is then applied, one finds that the integrated PVS is modified only by the convergence of horizontal fluxes of PVS. This provides a compact, intuitive description of PV evolution that does not suffer from the cancellation between diabatic and adiabatic terms found in the isobaric PV conservation equation (Haynes and McIntyre, 1987; Tory *et al*. 2012).

We are studying a system that is not approximately adiabatic, and in which the Coriolis parameter is small enough that any large deformation of isentropes (e.g. by a pulse of heating) is quickly relaxed by convergent mass fluxes. Thus, isobars and isentropes are nearly parallel and fixed in height, consistent with the weak temperature gradient (WTG) approximation (Sobel and Bretherton, 2000). The isentropic PVS therefore behaves like the isobaric absolute vorticity; both are much more bottom-heavy than PV (Figure 2b). The flux form of the absolute vorticity equation in pressure coordinates is isomorphic to Equation 2, with $\dot{\theta}$ replaced by the vertical velocity ω. Since ω is largely specified by $\dot{\theta}$ in low latitudes (e.g. Sobel and Bretherton, 2000), the evolution of PVS in isentropic coordinates is well-approximated by the evolution of absolute vorticity in pressure coordinates. Furthermore, in a formal WTG system, the PV conservation equation at each pressure level is proportional to the absolute vorticity equation (Sobel *et al*. 2001; Raymond *et al*. 2015).

Given all of this, in our subsequent analyses and idealized models we focus primarily on the evolution of PV in pressure coordinates and secondarily on absolute vorticity in pressure coordinates. This provides direct insight to the invertible Ertel's PV, connecting well with previous studies of PV in tropical vortices (e.g. Yu *et al*. 2010; Raymond, 2012; Yuan and Wang, 2014; Boos *et* *al*. 2015) as well as prior analyses of PV in isobaric coordinates (e.g. Raymond, 1992; Stoelinga, 1996; Yuan and Wang, 2014). As discussed above and in Section 5, PV is proportional to PVS and to absolute vorticity at each vertical level under WTG, but the difference in their vertical structures and budgets may be important in some circumstances, such as in regions of large background vertical wind shear. In such cases, strong lower-tropospheric horizontal flow below a stationary and positive PV anomaly isolated at upper levels would produce a stationary and positive absolute vorticity anomaly in the lower-tropospheric flow; the vorticity budget would exhibit large cancellation at low levels between horizontal advection and stretching by the induced vertical flow. This exact scenario was provided by Hoskins *et al*. (1985) as an example of the superior conceptual simplicity of PV over absolute vorticity, and was documented to occur in South Asian monsoon depressions by Boos *et al*. (2015).

4 RESULTS II: OBSERVATIONALLY ESTIMATED PV TENDENCIES

4.1 Diabatic PV tendencies

The conservation equation for Ertel's PV is

$$\frac{\mathrm{D}q}{\mathrm{D}t} = \frac{1}{\rho}\boldsymbol{\eta}\cdot\nabla\dot{\theta} + \frac{1}{\rho}(\nabla\times\mathbf{F})\cdot\nabla\theta, \quad (3)$$

where D/D*t* is the material derivative and F is the frictional force per unit mass. The terms on the right of Equation 3 are the diabatic PV generation and the PV tendency due to friction, respectively. When considering the storm-scale PV, friction can be neglected during the early stage of TD spin-up (e.g. Schubert and Alworth, 1987) because of weak surface winds. Indeed, Murthy and Boos (2018) found that the frictional spin-down tendency could be neglected in an approximate scaling for the intensification rate of TDs in an idealized model. We neglect PV tendencies due to friction in the remainder of this study.

As mentioned in Section 2, we use the YOTC reanalysis to obtain estimates of the diabatic heating tendencies due to radiation, cloud microphysics, shallow convection, and deep convection during TD spin-up (tendencies from turbulent diffusion and parametrized deep convection are summed and henceforth termed deep convection, as discussed above). We convert these into tendencies of potential temperature (i.e. $\dot{\theta}$), then calculate diabatic PV tendencies from the three-dimensional dot product of the absolute vorticity vector and the heating gradient.

We begin by examining the latent heating tendencies (Figure 3). Heating from parametrized cloud microphysics is positive above the melting level and negative below, qualitatively comparable to typical stratiform heating profiles. The associated diabatic PV generation peaks in the mid-troposphere and spans the melting level. The smaller peak magnitude of lower-tropospheric cooling leads to relatively weak, though more spatially extensive, diabatic PV destruction (this negative PV tendency has a magnitude smaller than that of the lowest contour shown in Figure 3a).

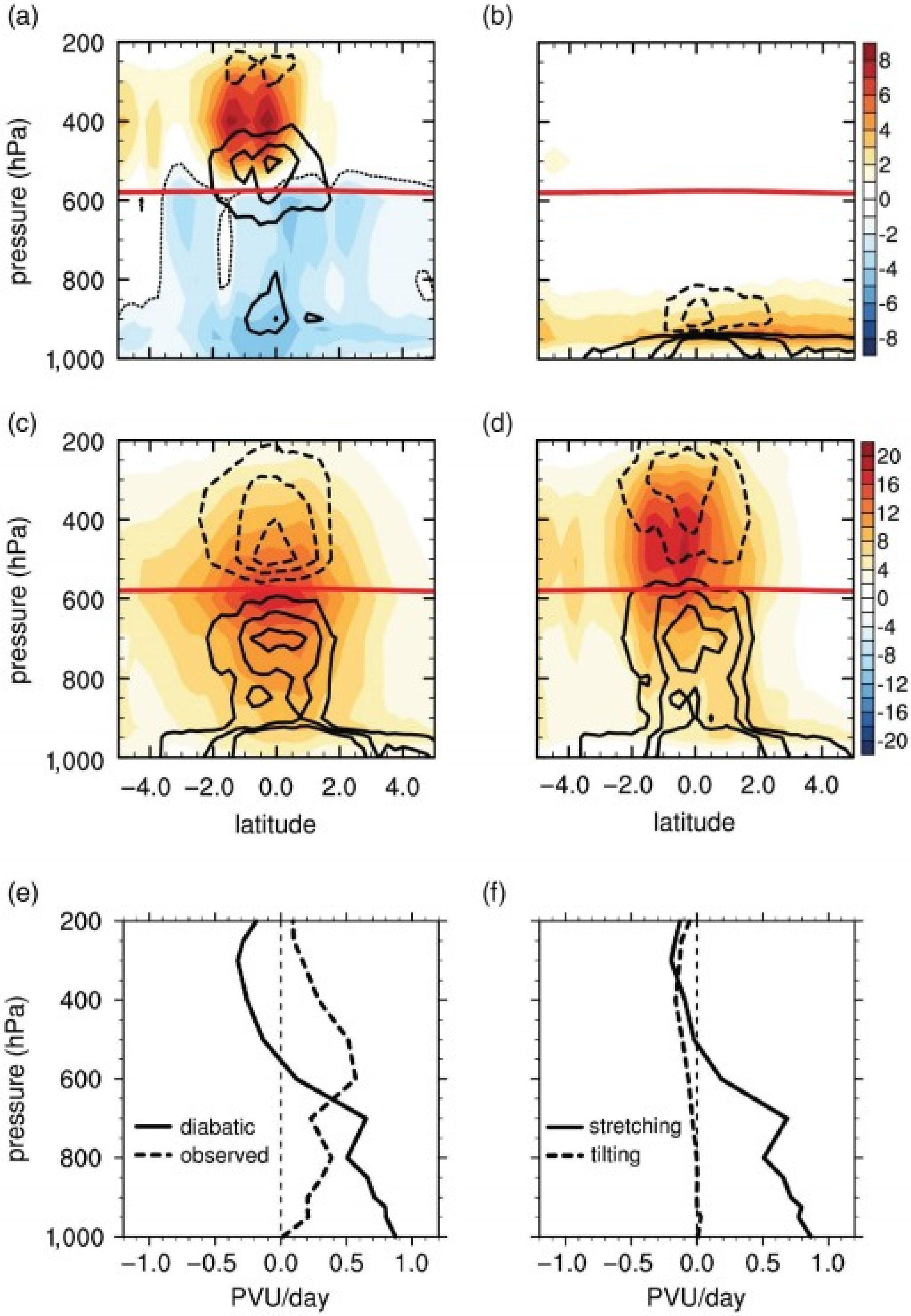

Figure 3. Top four panels show latitude–height cross-sections of the storm-centred composite mean diabatic heating tendency (K/day, colour shading) and diabatic PV tendency (contours with interval of 0.2 PVU/day) from (a) microphysics, (b) shallow convection, (c) deep convection, and (d) total, respectively. The nearly horizontal line at roughly 600 hPa indicates the 0°C melting level, as in Figure

2. In (a), the negative values of heating are enclosed by a thin dotted line. Note the change in colour scale between the top two panels and the lower two panels. (e) shows vertical profiles of the total diabatic (solid) and total observed Eulerian (dashed) PV tendencies. (f) shows vertical profiles of the stretching-like (solid) and tilting-like (dashed) diabatic tendencies (see Section 4.1 for details). Vertical profiles are obtained by horizontally averaging variables in a 5° × 5° box around the storm centre. (c) depicts the sum of diabatic heating from deep convection and turbulent diffusion, as discussed in Section 2

Diabatic heating by shallow convection occurs between the surface and 800 hPa, resulting in a vertical dipole of diabatic PV tendencies in this layer. This is consistent with Wang (2014), who found that shallow convection plays an important role during early TC genesis by spinning up a near-surface cyclonic circulation and moistening the lower troposphere. In contrast, latent heating in the deep convective parametrization (sum of deep convection and turbulent diffusion) is distributed throughout the troposphere, with maximum values near 600 hPa. As a result, the diabatic PV generation due to deep convection is bottom-heavy, with PV generated below and destroyed above 600 hPa. Furthermore, deep convective heating is several times larger in magnitude than stratiform heating (note the change in scale in Figure 3a,c), consistent with the dominant role of deep convection in our general understanding of TC intensification and genesis (e.g. Emanuel, 2003; Montgomery and Smith, 2017). Indeed, the significance of widespread deep convection has been documented during all stages of TC intensification, including genesis (e.g. Hendricks *et al*. 2004; Houze *et al*. 2009). However, more recent studies have found an increase in stratiform precipitation during TC intensification (Wang *et al*. 2010; Tao *et al*. 2017), which can be attributed to an increase in the horizontal extent of stratiform convection as intensification proceeds (Fritz *et al*. 2016; Yang *et al*. 2018). Stratiform convection is typically associated with the creation of a mid-level vortex, which some studies consider essential for the subsequent formation of a low-level incipient TC (e.g. Bister and Emanuel, 1997; Raymond and Sessions, 2007). While it has been hypothesized that this mid-level vortex creates a conducive environment for efficient vortex stretching by deep convection (Wang *et al*. 2010), a detailed examination of the adiabatic and diabatic PV tendencies associated with stratiform and deep convection during TC intensification has not been performed. The rest of this study is devoted to examining these tendencies in TDs.

In the composite mean, radiative temperature tendencies are weak and relatively uniform in the vertical, approximately −2 K/day at the TD periphery and −1 K/day at the centre (not shown). This produces diabatic PV tendencies of magnitude smaller than 0.05 PVU/day, an order of magnitude smaller than tendencies from phase changes of water. We conclude that diabatic PV generation by cloud–radiation interactions is negligible in this reanalysis, and that these interactions are perhaps more important during earlier stages of spontaneous TC genesis when moist convection self-aggregates in cloud-system resolving numerical simulations (e.g. Khairoutdinov and Emanuel, 2013; Wing *et al*. 2016; Muller and Romps, 2018).

The total diabatic heating closely resembles the heating due to deep convection, with the altitude of maximum heating elevated above the melting level due to heating from cloud microphysics (Figure 3d), consistent with observations of mesoscale convective systems (e.g. Houze, 1997). As a consequence, the total diabatic PV generation resembles the bottom-heavy PV generation due to deep convection, with positive values below and negative values above 600 hPa. Thus, even though the diabatic PV generation by stratiform heating peaks in the mid-troposphere, the total diabatic PV generation is bottom-heavy and does not resemble the mid-level PV maximum (Figure 2). This is confirmed when vertical profiles of diabatic PV generation and the Eulerian time tendency of PV in TDs are compared (Figure 3e). Relative to the initial pre-TD state, the composite mean PV increases primarily at mid-levels, near 550 hPa, whereas diabatic PV generation is positive only below 600 hPa and peaks at the surface. This illustrates, for the particular context of TDs, the more general near-cancellation of diabatic and adiabatic PV tendencies (e.g. Haynes and McIntyre, 1987; Tory *et al*. 2012).

While these diabatic PV tendencies were computed using the three-dimensional dot product of η and $\nabla\dot{\theta}$, some previous studies considered the product of vertical components of these vectors to dominate (e.g. Houze *et al*. 2009). We examine the relative contributions of the horizontal and vertical components of the dot product by expressing the diabatic PV tendency as

$$\frac{1}{\rho}\boldsymbol{\eta}\cdot\nabla\dot{\theta} = g\left[\boldsymbol{\eta}_{\mathrm{h}}\cdot\nabla_{h}\dot{\theta} - \eta_{p}\frac{\partial\dot{\theta}}{\partial p}\right], \quad (4)$$

where $\eta_{\mathrm{h}} = (\partial_p v, -\partial_p u)$ is the horizontal component of absolute vorticity obtained after neglecting horizontal gradients of vertical velocity, $\eta_p = \zeta + f$ is the vertical component of absolute vorticity, and $\zeta = \partial_x v - \partial_y u$ is the vertical component of relative vorticity. The first term on the right represents diabatic PV generation due to tilting of the horizontal absolute vorticity by the horizontal gradient of heating, and is henceforth called the “tilting-like” diabatic PV tendency. The second term on the right is the diabatic PV generation due to vertical components of absolute vorticity and heating gradient, and is hencefoth referred to as the “stretching-like” diabatic PV tendency.

The ratio of the magnitudes of the stretching-like and tilting-like diabatic PV tendencies can be shown to be

$$\frac{\left|(\zeta+f)\frac{\partial\dot{\theta}}{\partial p}\right|}{|\boldsymbol{\eta}_{\mathrm{h}}\cdot\nabla_{\mathrm{h}}\dot{\theta}|} \simeq 1 + \frac{1}{Ro}, \quad (5)$$

where $Ro = \zeta/f$ is the Rossby number. Thus, the stretching-like tendency is much larger than the tilting-like tendency only when $Ro \ll 1$, and the two terms are comparable when $Ro \gg 1$.

In the composite mean, TDs have an approximate ζ of $10 \times 10^{-5} s^{-1}$ (contours in Figure 2), which is roughly twice the planetary vorticity at the composite mean storm centre of 20°N latitude. This gives $Ro \approx 2$, so the contribution of the tilting-like diabatic PV tendency cannot be neglected. When vertical profiles of stretching-like and tilting-like diabatic PV tendencies are compared explicitly, the two are nearly equal in the upper troposphere (Figure 3f). The tilting-like tendency is negative above 600 hPa, consistent with a mid-level vortex with peak winds near 800 hPa that also has strong horizontal gradients of heating in the middle- and upper-troposphere (shading above the melting level in Figure 3d).

4.2 Comparison of YOTC heating with TRMM

We now compare the YOTC heating tendencies for one particular TD on 25 September 2008 with heating rates obtained from TRMM. This storm was chosen because the TRMM swath passed through the centre of the storm within an hour of the best-track time step while also covering 55% of the 5° × 5° box surrounding the storm centre. At 600 hPa, which is near the melting level, PV peaks near the storm centre, with some secondary maxima to the northeast (contours in Figure 4).

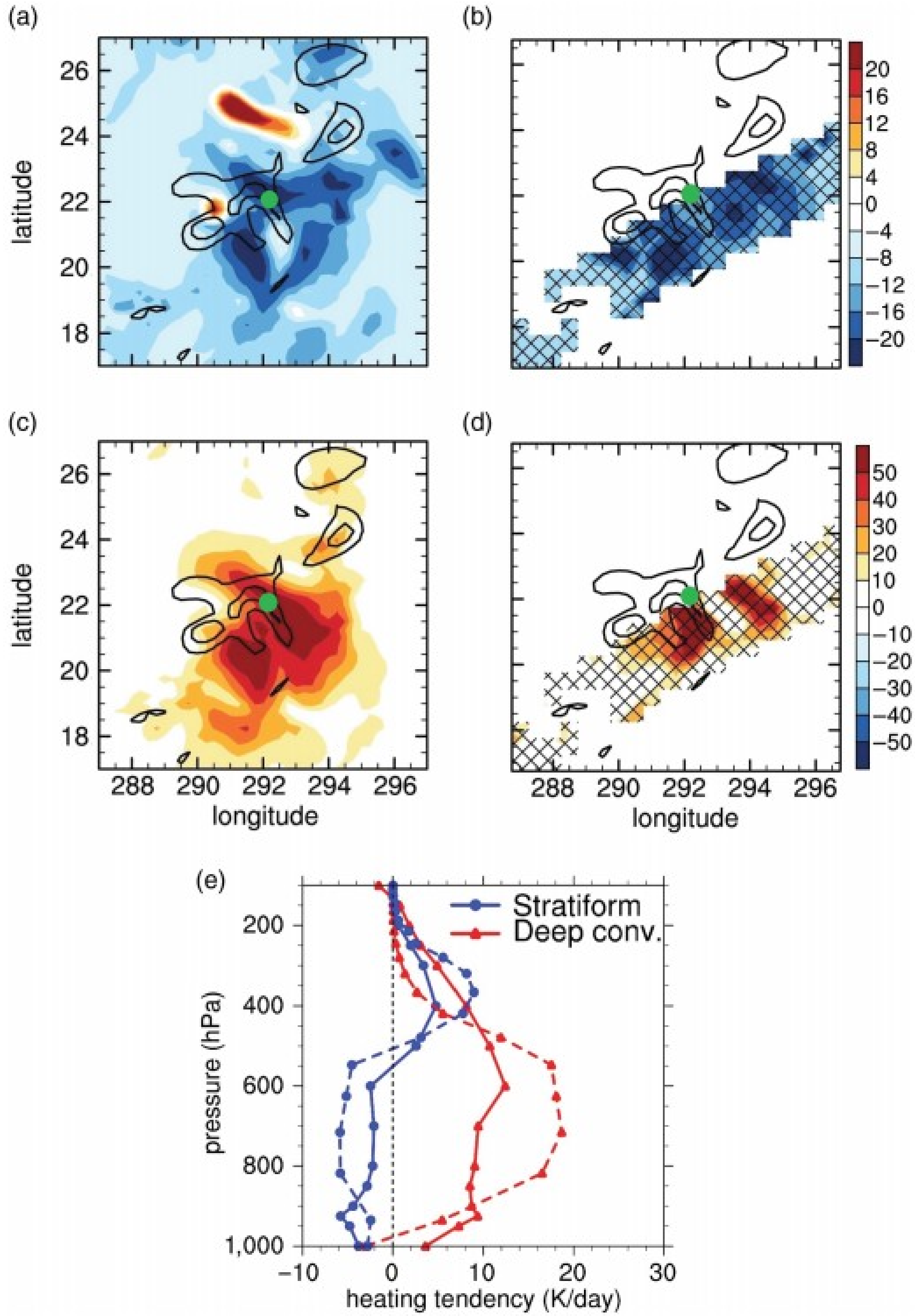

Figure 4. (a)–(d) show storm-centred horizontal sections at 600 hPa of heating tendencies (K/day, colour shading) in one case-study (0000 UTC 25 September 2008) from (a) YOTC microphysics, (b) TRMM stratiform, (c) YOTC deep convection, and (d) TRMM deep convection. In these panels, contours show the PV at 600 hPa for reference, and hatching in (b) and (d) depict the TRMM swath where data are available. Note the change in colour scale between the top two panels and the lower two panels. (e) shows the composite mean vertical profiles (only storms captured by TRMM) of deep convective

and stratiform heating profiles from both YOTC (solid) and TRMM (dashed), which are obtained by horizontally averaging variables only in the region where TRMM data are available within a 5° × 5° box around the storm centre. Small circle in (a)–(d) depicts the TD centre.

The YOTC heating tendencies from deep convection are large near the storm centre, with peak values exceeding 70 K/day (Figure 4). At 600 hPa, this deep convective heating is collocated with cooling from the cloud microphysics scheme, capturing the melting of precipitating ice. There are a few regions of positive microphysics heating north of the storm centre at 600 hPa, and the microphysics heating is more uniformly positive at 400 hPa (not shown). The microphysics scheme also produces small regions of strong heating in the lower troposphere (with magnitude 50 K/day and area 0.5° × 0.5°, not shown); these are presumably caused by grid-scale updraughts (e.g. Houze *et al*. 2009).

The TRMM swath passes southeast of the storm centre, but nevertheless captures the regions of stratiform cooling and deep convective heating. The magnitude of the TRMM-derived heating rates is comparable to that of the YOTC rates, supporting our interpretation of the YOTC microphysics and deep convective heatings as stratiform and deep convective modes, respectively. Comparison of vertical profiles of stratiform and deep convective heating in the storm-centred composite of eligible storms in YOTC and TRMM (Figure 4e) further reinforces their similarities, although some differences exist. Each component of the TRMM-derived heating is larger in peak magnitude than the corresponding YOTC profile, but there is some cancellation between these differences so that the sum of the deep convective and stratiform heating rates is more similar between TRMM and YOTC. Overall, the diabatic PV generation computed using the TRMM heating profiles is qualitatively similar to that computed from YOTC (not shown).

4.3 Net PV tendencies

We now examine the net Eulerian rate of change of PV, expanding the material derivative,

$$\frac{\partial q}{\partial t} = \frac{1}{\rho}\boldsymbol{\eta} \cdot \nabla\dot{\theta} - \mathbf{u}_{\mathrm{h}} \cdot \nabla_{\mathrm{h}} q - \omega\frac{\partial q}{\partial p}, \quad (6)$$

where u_h is the horizontal wind, Δ_h is the horizontal gradient, and ω is the vertical velocity in pressure coordinates. The horizontal mean horizontal wind in a 5° × 5° box around the storm centre is subtracted from u_h before computing the horizontal advective tendencies, a practice commonly used to remove tendencies associated with horizontal propagation of vortices (e.g. Tory *et al*. 2012). Because we do this at each vertical level, this also removes any tilting of the PV column from vertical changes in the horizontal mean u_h. The horizontal and vertical advection computed from YOTC data is noisy, even in the composite mean, so we limit discussion to their horizontally averaged vertical profiles (Figure 5, with horizontal and vertical advection equal to $-u_h \cdot \Delta_h q$ and $-\omega \partial_p q$, respectively, and diabatic PV generation plotted for reference).

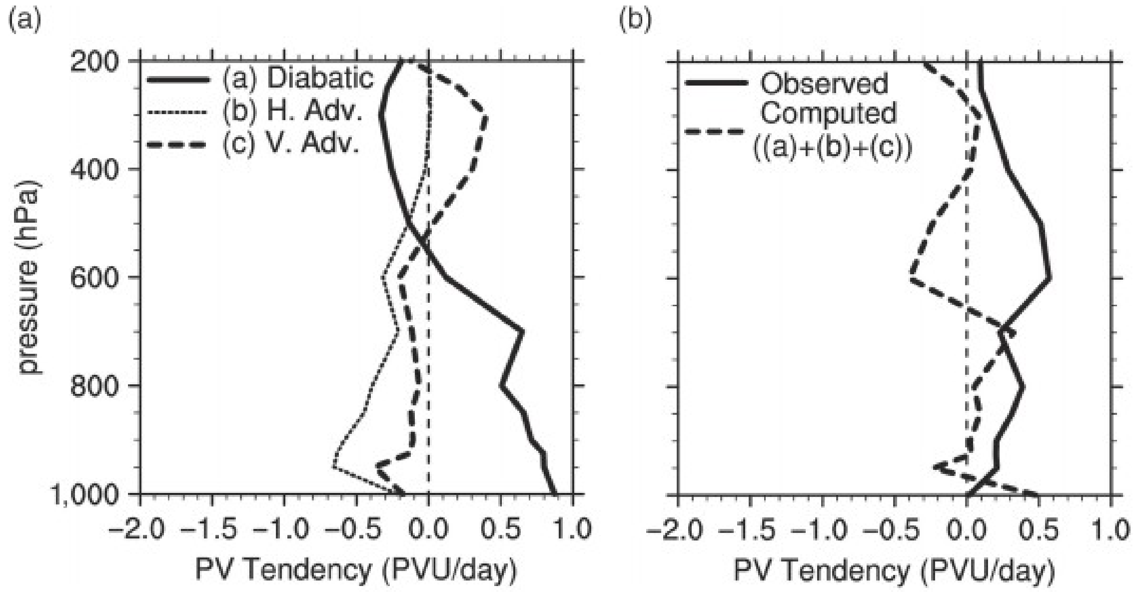

Figure 5. Storm-centred vertical profiles of (a) terms in the Eulerian PV budget, and (b) comparison of the computed and observed PV tendencies. Vertical profiles are obtained by horizontally averaging variables in a 5° × 5° box around the storm centre

Vertical advection transports PV from the lower and middle troposphere to the upper troposphere, as it does in mature TCs (e.g. Schubert and Alworth, 1987). Horizontal advection is negative in the middle and lower troposphere and vanishes in the upper troposphere. The symmetric, tangential component of the horizontal wind is expected to make only a small contribution to this horizontal advection, with the radial secondary circulation advecting low-PV air from the periphery of the TD. There is strong cancellation between diabatic and adiabatic PV tendencies, as discussed by Tory *et al*. (2012).

However, the computed sum of diabatic and adiabatic PV tendencies does not equal the Eulerian PV tendency in YOTC, with PV budget residuals being large (Figure 5b), especially in the mid-troposphere where the PV maximum occurs. The large residues are perhaps due to the use of different numerical methods and coordinate systems from those used in the YOTC model (e.g. Seager and Henderson, 2013), and due to the non-conservative analysis tendencies. This lack of closure of the PV budget, even in the horizontally averaged composite mean, motivates construction of an idealized model to better understand controls on the vertical structure of PV.

5 RESULTS III: IDEALIZED MODELS

5.1 Weak temperature gradient approximation

A localized pulse of heating imposed on a fluid in a balanced state will displace isentropes and thus instantaneously modify q without changing η; subsequent adjustment of the fluid back to balance relaxes the isentropes toward their initial positions and creates a vorticity anomaly of the same sign as the heating-induced q perturbation (Hoskins *et al*. 1985; Haynes and

McIntyre, 1987). In low latitudes, the deformation radius is large enough that isentropes are to leading-order horizontal. Sobel and Bretherton (2000) formalized this in the Weak Temperature Gradient (WTG) approximation, in which diabatic heating is balanced by the adiabatic cooling of ascent, that is, $\omega\partial_p\theta = \dot{\theta}$. The θ anomalies needed to maintain thermal wind balance are obtained as diagnostic, second-order corrections from the heating-induced circulation. Under WTG, PV dynamics simplify because of the nearly horizontally homogeneous θ distribution, with the governing PV equation becoming proportional to the absolute vorticity equation (Raymond *et al*. 2015) and the WTG form of PV becoming

$$q_w = gs\eta_p \quad (7)$$

with $s = -\partial_p\theta$. As discussed by Sobel *et al*. (2001), PV and the vertical component of absolute vorticity track the same quantity under WTG, with differences in their vertical structure due entirely to vertical variations of s. For our composite TD, q_w computed from the monthly mean s is only about 15% weaker than the full q, with a clear 500 hPa maximum (Figure 6). For this reason, we use our idealized models to study the evolution of q_w in a TD, choosing the conceptual simplicity of the WTG framework over the exactness of a primitive equation model. This approach is supported by studies of the PV changes that occur in models of cyclogenesis forced by imposed heatings, with the PV distribution in the final balanced state being independent of variations in or details of the adjustment process (Delden, 2003). To be clear, the WTG approximation is employed here only to understand how the storm-scale vertical structure of TDs evolves over periods of 1–2 days given a specified diabatic heating. We do not expect WTG to hold on much finer temporal scales, and we do not use it to understand how convection within a TD responds to balanced temperature anomalies. In YOTC, the TDs have temperature anomalies around 1 K in magnitude relative to the surroundings (not shown), consistent with Zawislak and Zipser (2014a); the presence of these anomalies does not invalidate WTG, as they can be recovered diagnostically from the diabatically driven circulation and in the scaling simply play a secondary role in the thermodynamic equation compared to vertical advection and diabatic heating.

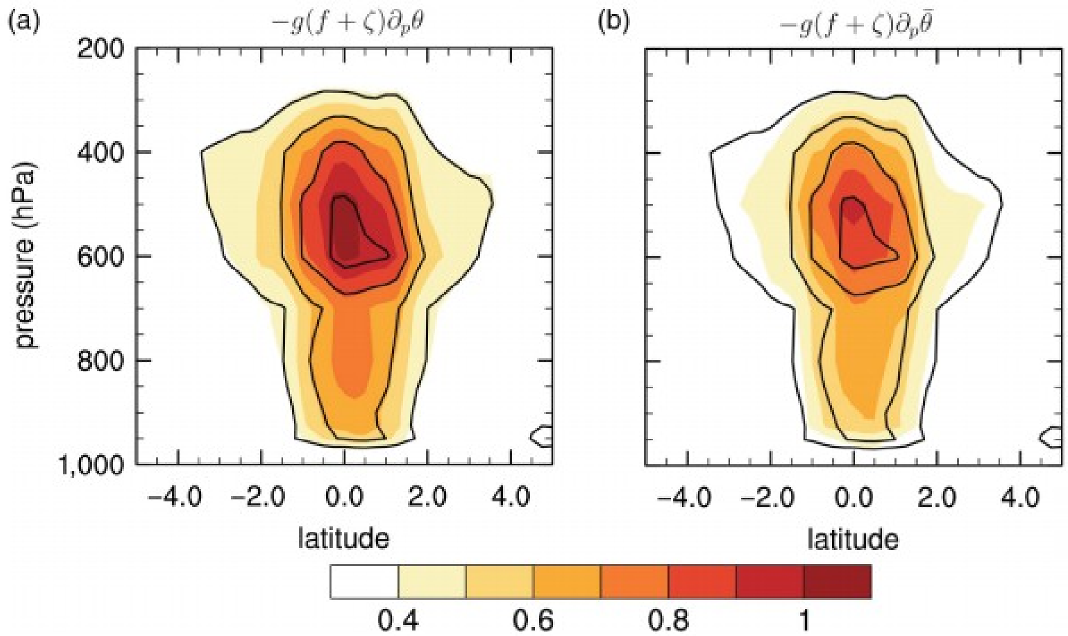

Figure 6. In (a), the storm-centred meridional cross-section of PV is computed using only the vertical components of absolute vorticity and potential temperature gradient (PVU, colour shading). In (b), a time-mean quantity of vertical potential temperature gradient is instead used to compute PV (PVU, colour shading). The time-mean quantity is the monthly mean computed using data from 2008 and 2009. In both panels, contours (interval of 0.2 PVU) indicate composite mean PV for reference

The WTG approximation can only be used for TDs of sufficiently small scale and amplitude. Sobel *et al*. (2001) showed from a shallow-water scaling that WTG holds when

$$Ro\left(\frac{L}{L_{\mathrm{R}}}\right)^2 \ll 1, \quad (8)$$

where L is the disturbance length-scale, taken here to be 250 km for a TD, and $L_{\mathrm{R}} = NH/f$ is the Rossby deformation radius, equal to 2,000 km at a latitude of 20° with a disturbance height of $H = 10$ km and a buoyancy frequency of $N = 10^{-2}\mathrm{s}^{-1}$. Satisfying Equation 8 requires $\zeta \leq 30 \times 10^{-5} s^{-1}$.

Use of WTG requires specification of a stratification s. We specify an idealized profile of s that is linear in pressure and approximates the observed composite mean static stability (Figure 7). Our idealized profile is not a best-fit line, but instead aims to represent observed values in the lower and middle troposphere, where peak PV values lie.

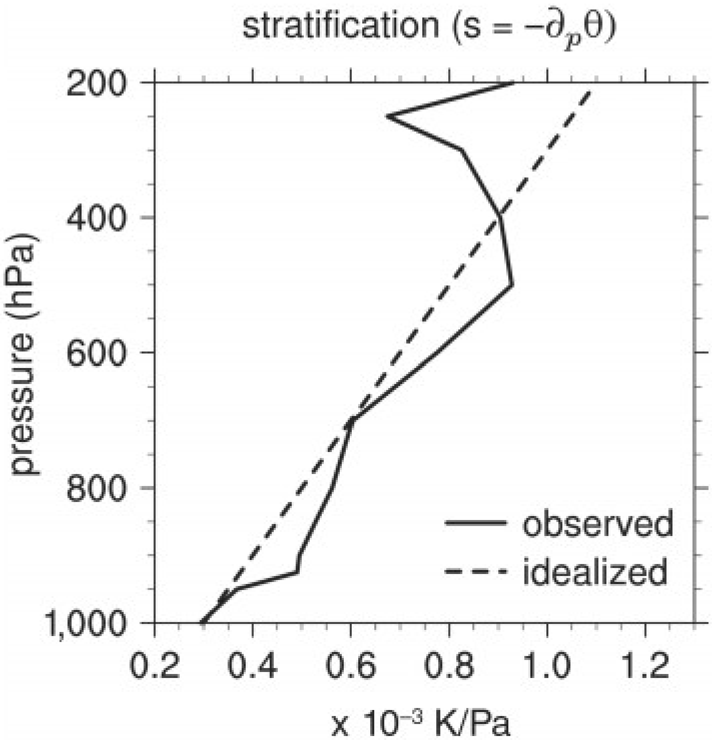

Figure 7. Vertical profiles of observed (solid) and idealized (dashed) static stability, $s = -\partial\theta/\partial p$. The observed vertical profile is obtained by horizontally averaging the storm-centred composite mean in a 5° × 5° box

We also specify time-invariant diabatic heatings, in order to more clearly understand how different vertical profiles of heating lead to combined diabatic and adiabatic (i.e. advective) PV tendencies. During real-world TD spin-up, the diabatic heating varies with the circulation, perhaps via wind-induced changes in surface enthalpy fluxes (Murthy and Boos, 2018), but we limit our focus to understanding the diabatic and adiabatic PV tendencies caused by canonical stratiform and deep convective profiles of heating (e.g. Houze, 1997). The stratiform profile, specified as a sinusoid between 1,000 and 100 hPa with peak amplitude of 6 K/day, is positive above 550 hPa and negative below. The deep convective profile, specified as half a sinusoid with peak amplitude equal to 16 K/day, is positive throughout the troposphere with a maximum at 550 hPa (Figure 8). The superposition of deep convective and stratiform heating is positive at all levels, with a maximum at 400 hPa. These idealized profiles are similar in both amplitude and qualitative vertical structure to the TRMM convective and stratiform profiles, but the TRMM profiles are more bottom-heavy.

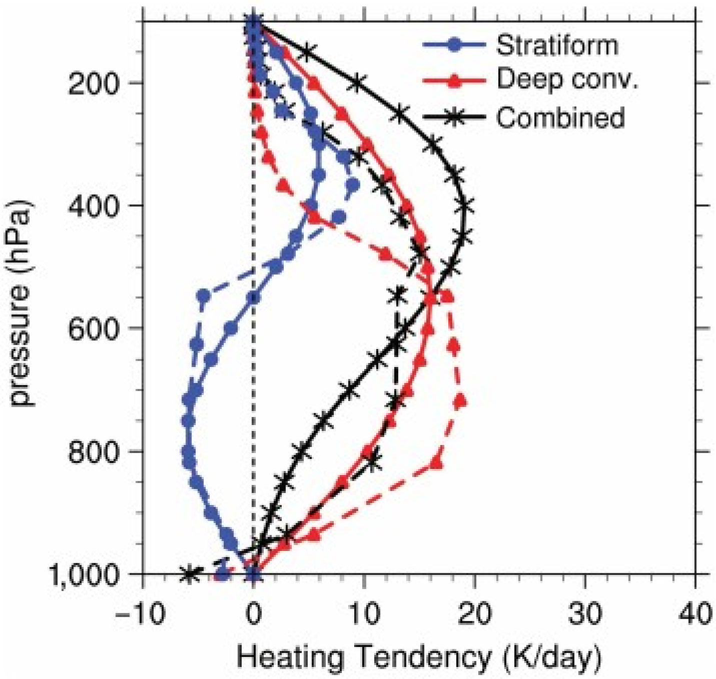

Figure 8. Vertical profiles of idealized (solid) and TRMM (dashed) heating (K/day), in deep convective and stratiform clouds. The combined heating profile is a linear combination of the deep convective and stratiform profiles

5.2 1D flux form model

Since PV in the WTG framework is proportional to absolute vorticity (e.g. Raymond *et al*. 2015), it seems plausible that the flux form of the relevant conservation equation might provide a more concise understanding of the evolution of PV (as in Haynes and McIntyre, 1987). Here we develop a 1D model for the evolution of PV in a cylindrical region with a radius equal to R_Q, with $\dot{\theta}$ positive and horizontally uniform for radii $r < R_Q$, and $\dot{\theta} = 0$ at $r = R_Q$. We take the inviscid isobaric absolute vorticity equation in flux form (Haynes and McIntyre, 1987),

$$\frac{\partial \eta_p}{\partial t} = -\nabla \cdot \left[\mathbf{u}_h \eta_p + \omega \boldsymbol{\eta}_h\right], \quad (9)$$

multiply this by g and the background stratification, then horizontally average within the cylindrical region of positive heating. Under WTG, the heating specifies the vertical motion, with $\omega = -\dot{\theta}/s$. On the boundary of the cylinder, we thus have $\omega = 0$ where $\dot{\theta} = 0$, so the convergence of the non-advective flux (the second term in Equation 9) is zero in the resulting horizontally averaged equation,

$$\frac{\partial \overline{q_w}}{\partial t} = -\overline{\nabla \cdot (\mathbf{u}_h q_w)}, \quad (10)$$

where an overbar denotes an average over the cylindrical heated region.

Applying the divergence theorem to the right-hand side of Equation 10,

$$-\overline{\nabla \cdot (\mathbf{u}_h q_w)} = \frac{-2u_r(R_Q)q_w(R_Q)}{R_Q}, \quad (11)$$

where u_r is the radial velocity, and $u_r(R_Q)$ and $q_w(R_Q)$ denote values of u_r and q_w at $r = R_Q$. Assuming that the azimuthal velocity is non-divergent and using the WTG constraint on ω, we can integrate the mass continuity equation in cylindrical coordinates,

$$\frac{1}{r}\frac{\partial(ru_r)}{r} + \frac{\partial\omega}{\partial p} = 0. \quad (12)$$

to obtain $u_r(r) = -r\partial_p\dot{\theta}/2$ for $r \leq R_Q$. The time tendency of q_w averaged over the heated region is then

$$\frac{\partial\overline{q_w}}{\partial t} = -q_w(R_Q)\frac{\partial}{\partial p}\left(\frac{\dot{\theta}}{s}\right). \quad (13)$$

A central question is how $q_w(R_Q)$ relates to $\overline{q_w}$. In a shallow-water system, Sobel *et al*. (2001) found that the axisymmetric WTG response to a cylindrical, top-hat heating had radially uniform relative vorticity within the heated region. If we similarly assume that q_w is radially uniform for $r \leq R_Q$, either because such a solution is exact for certain parameter values or because azimuthally asymmetric eddies not explicitly represented in our system relax q_w to such a radially uniform profile, then $q(R_Q) = \overline{q_w}$ and our 1D model becomes

$$\frac{\partial\overline{q_w}}{\partial t} = -\overline{q_w}\frac{\partial}{\partial p}\left(\frac{\dot{\theta}}{s}\right). \quad (14)$$

The horizontally averaged PV thus undergoes exponential growth when $\dot{\theta}/s$ increases with height, and exponential decay when it decreases.

The right-hand side of Equation 14 can be expanded to illustrate the explicit roles of diabatic PV generation and adiabatic vertical advection,

$$\frac{\partial\overline{q_w}}{\partial t} = -g\overline{\eta_p}\frac{\partial\dot{\theta}}{\partial p} - g\overline{\eta_p}\omega\frac{\partial s}{\partial p}. \quad (15)$$

The first term on the right is the stretching-like diabatic PV tendency (i.e. the last term in Equation 4), while the second term can be identified as the component of vertical PV advection not cancelled by the tilting-like diabatic PV tendency (compare with Equation 6, noting that horizontal advection is zero for $r < R_Q$ since horizontal gradients are zero there). As discussed by Haynes and McIntyre (1987) and Tory *et al*. (2012), there is strong but incomplete cancellation between adiabatic advection and diabatic generation terms in the advective form of the PV conservation equation, and the right-hand side of Equation 15 represents the residual in the WTG system under the assumption of horizontally uniform q_w in the heated region.

We numerically integrate Equation 14 on a 1D grid for 2 days of simulated time, with a vertical resolution of 1 hPa between 1,000 and 100 hPa, and a time-step of 10 s, using second-order centred finite differences. We also decompose the time tendencies using Equation 15.

For both stratiform and deep convective heating profiles, the stretching-like diabatic term dominates while the sum of vertical advection and the tilting-like diabatic term is relatively small (Figure 9). Over the course of two days, stratiform heating thus produces mid-level maxima in PV and absolute vorticity, while deep convective heating produces very bottom-heavy structures of PV and absolute vorticity. The superposition of deep convective and stratiform heating produces PV that is nearly uniformly in height below 600 hPa together with a bottom-heavy structure of vorticity. Although the PV maximum is thus elevated compared to the vorticity maximum, both are substantially more bottom-heavy than the structures seen in the composite TD based on YOTC data. This does not seem to be because of a bias in the heating or the diabatic PV tendencies: the stretching-like diabatic term is similar to that estimated from YOTC (compare diabatic PV tendency in Figure 9e with solid line in Figure 3f). The sum of vertical advection and the tilting-like term is also qualitatively similar to YOTC estimates (compare vertical advection in Figure 9e with sum of dashed line in Figure 3f and dashed line in Figure 5a). The absence of surface friction could make the PV too bottom-heavy in the idealized model, although surface friction has often been neglected during the early stage of TD spin-up in models for the storm-scale evolution of PV (e.g. Schubert and Alworth, 1987). We instead focus on the absence of horizontal advection in our 1D model as a more likely cause of its differences with the YOTC composite. Horizontal advection is zero in the 1D model because of our questionable assumption that PV is radially uniform within the heated region; this may be accurate above the heating maximum where flow diverges (and indeed is an exact solution in that divergent region under WTG, as shown by Sobel *et al*. (2001)), but below the heating maximum the inward flow will reduce PV toward that of the environment at $r = R_Q$. This is expected when one considers that PVS is expected to be concentrated in regions of horizontal convergence (Haynes and McIntyre, 1987). Relating $q_w(R_Q)$ to $\overline{q_w}$ requires solving for the time-evolving radial structure of q_w, which in turn requires going from a 1D to a 2D model.

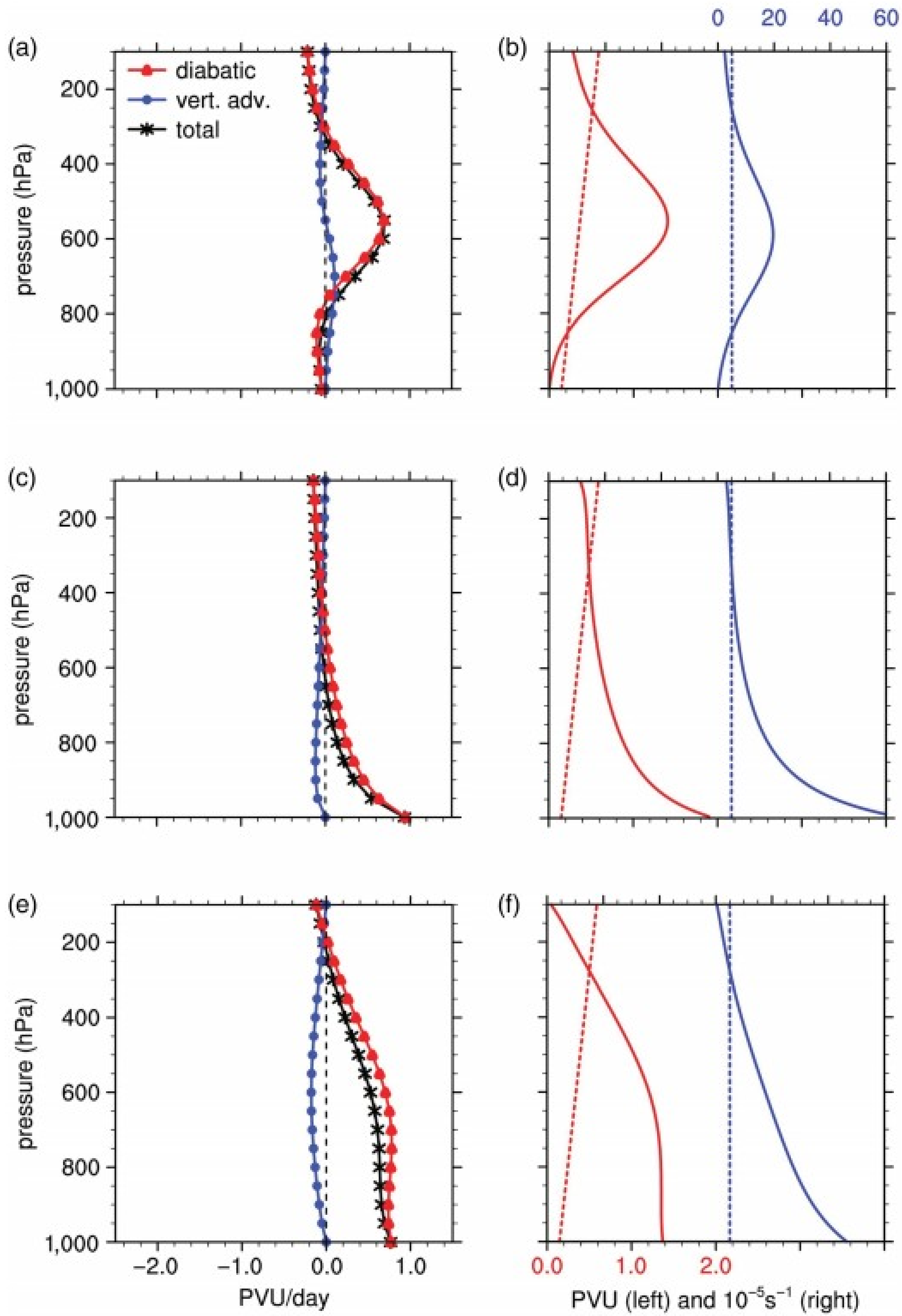

Figure 9. The vertical profiles of (a, c, e) PV tendencies and (b, d, f) PV (left) and absolute vorticity (right) in the 1D model in response to (a, b) stratiform, (c, d) deep convective, and (e, f) combined heating. The PV tendencies are temporally averaged during the first 2 days and the PV and absolute vorticity profiles are shown at the end of day 2. The dashed lines in (b, d, f) are the PV and planetary vorticity of the unperturbed environment

5.3 2D axisymmetric model

The axisymmetric, time-invariant heating is now specified as

$$\dot{\theta}(r,p) = \begin{cases} Q(p) & \text{for } r < R_Q, \\ \gamma(p) & \text{for } R_Q < r < R, \\ 0 & \text{for } r > R, \end{cases} \quad (16)$$

where $Q(p)$ is the deep convective, stratiform, or combined heating profile (Figure 8), and

$$\gamma(p) = \frac{-Q(p)R_Q^2}{R^2 - R_Q^2} \quad (17)$$

is the cooling that balances the prescribed heating. We choose $R_Q = 250$ km and $R = 2{,}500$ km.

In cylindrical coordinates, the axisymmetric PV equation is

$$\frac{\partial q_w}{\partial t} = -\frac{q_w}{s}\frac{\partial \dot{\theta}}{\partial p} + g\frac{\partial u_\phi}{\partial p}\frac{\partial \dot{\theta}}{\partial r} - u_r\frac{\partial q_w}{\partial r} - \omega\frac{\partial q_w}{\partial p}, \quad (18)$$

where u_φ is the azimuthal velocity. The terms on the right of Equation 18 are the stretching-like and tilting-like diabatic PV tendencies, radial advection, and vertical advection, respectively. The partial cancellation between the tilting-like diabatic tendency and vertical advection that occurred in the 1D model is not explicit here because we have not horizontally averaged.

As in the 1D model, we obtain u_r by integrating the mass continuity equation, obtaining

$$u_r(r) = \begin{cases} -\frac{r}{2}\frac{\partial \dot{\theta}}{\partial p} & \text{for } r < R_Q, \\ -\frac{r}{2}\frac{\partial \dot{\theta}}{\partial p}\left[1 - \frac{R^2}{r^2}\right] & \text{for } R_Q < r < R, \\ 0 & \text{for } r > R. \end{cases} \quad (19)$$

The azimuthal velocity is obtained by numerically integrating the relative vorticity ζ in r, with

$$\zeta = \frac{1}{r}\frac{\partial (r u_\phi)}{\partial r}. \quad (20)$$

Equation 18 is solved on an axisymmetric grid of radial resolution 1 km extending out to 3,000 km, vertical resolution of 1 hPa between 1,000 and 100 hPa, and a time-step of 1 s. Vertical and radial derivatives in the diabatic PV tendencies are computed using second-order, centred finite differences, while horizontal and vertical advection are computed using a second-order upwind scheme. Similar to the 1D model, we integrate for two days of simulated time.

Although we intend the heating to have a “top-hat” structure in radius, we linearly transition between $Q(p)$ and $\gamma(p)$ over a radius of 10 km just inside r

$= R_Q$ to prevent numerical instabilities. The tilting-like diabatic PV tendency thus only exists for radii 10 km inside of R_Q. We plot the stretching-like and tilting-like diabatic PV tendencies together, because they can be easily distinguished by their contrasting radial distributions.

For stratiform heating, the time-mean stretching-like diabatic PV tendency is concentrated near the storm centre in the mid-troposphere, with a weak negative tendency below 800 hPa (Figure 10a). Ascent and descent in the upper and lower troposphere, respectively, vertically advect PV down-gradient, countering the weak diabatic tendencies there (Figure 10c). Mid-tropospheric convergence horizontally advects lower PV into the heated region, reducing the radius of the PV and absolute vorticity distributions compared to that of the heating (Figure 10b). The total (diabatic plus adiabatic) PV tendency caused by stratiform heating is mostly restricted to a radius of 150 km and peaks at 550 hPa (Figure 10d). After two days, PV and absolute vorticity have similar radial and vertical structures, peaking near 600 hPa as in the 1D model (Figure 10e,f). The tilting-like diabatic tendency consists of a narrow annulus of largely negative values just inside $r = R_Q$, with positive values in layers where the vertical gradient of heating changes sign (Figure 10a). The PV generated in this annulus is advected by radial and vertical circulations, making only a meagre contribution to the total PV tendency near the heating boundary.

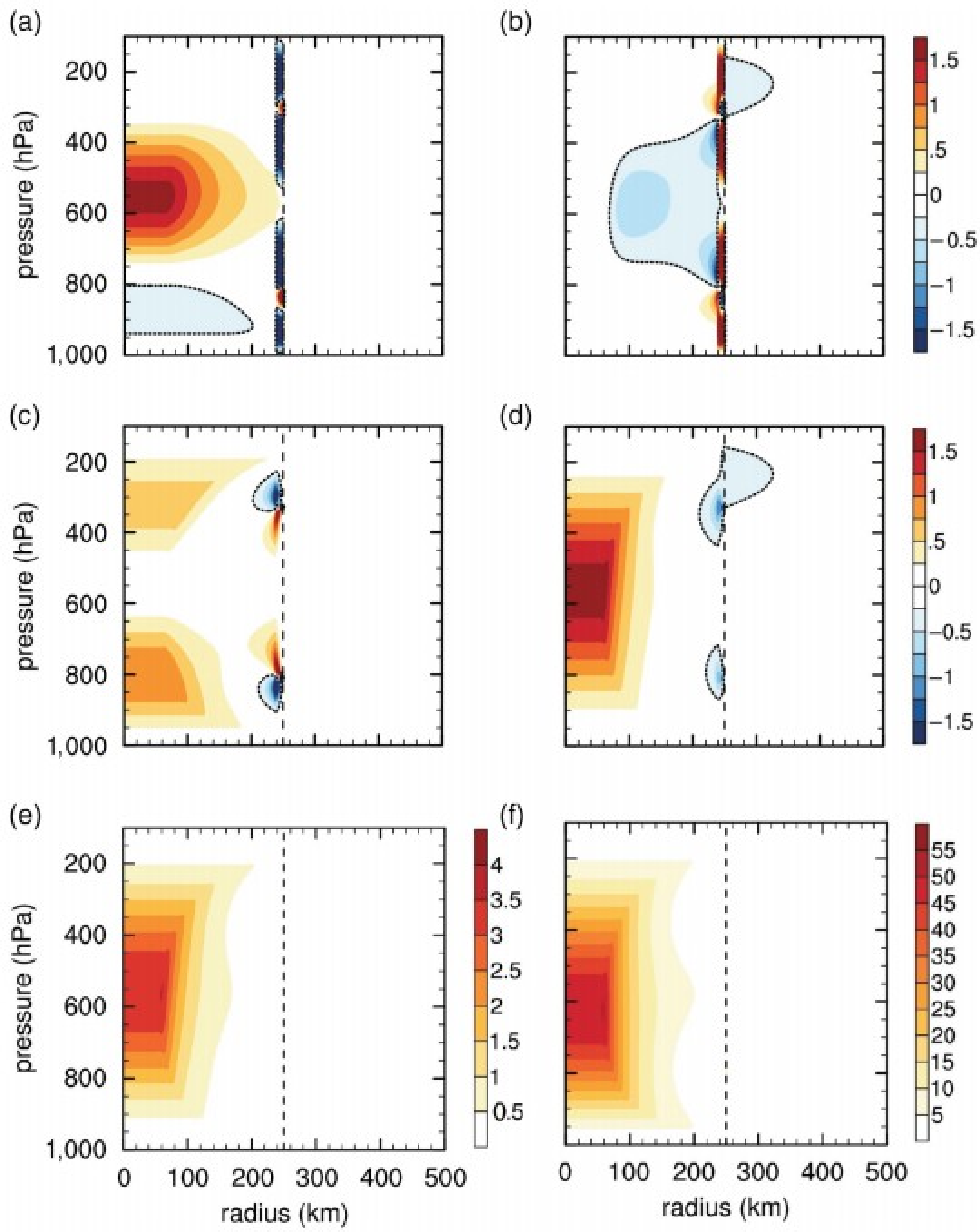

Figure 10. Time-averaged (a) diabatic PV tendency, (b) horizontal advection, (c) vertical advection, and (d) total PV tendency (all PVU/day) during the first 2 days of the axisymmetric 2D model in response to stratiform heating. Diabatic PV tendency includes both stretching-like and tilting-like tendencies, with the tilting-like tendency radially restricted to 10 km near the heating boundary. Negative PV tendencies are enclosed by a thin dotted line. Lowest panels depict the (e) PV (PVU) and (f) absolute vorticity ($10^{-5}s^{-1}$) on day 2. The vertical dotted line in all panels indicates the radius ($r = 250$ km) within which the heating is applied

Analogous behaviour holds for deep convective heating, with the stretching-like diabatic tendency and the total tendency peaking at the surface (Figure 11). Radial advection again reduces the radial extent of the total PV tendency to roughly 150 km, and the heating-induced full-tropospheric ascent deepens the positive PV tendency through vertical advection. The spatial distributions of PV and absolute vorticity are again similar; their vertical structures resemble those of the 1D model, but their radial scales are greatly reduced by radial advection.

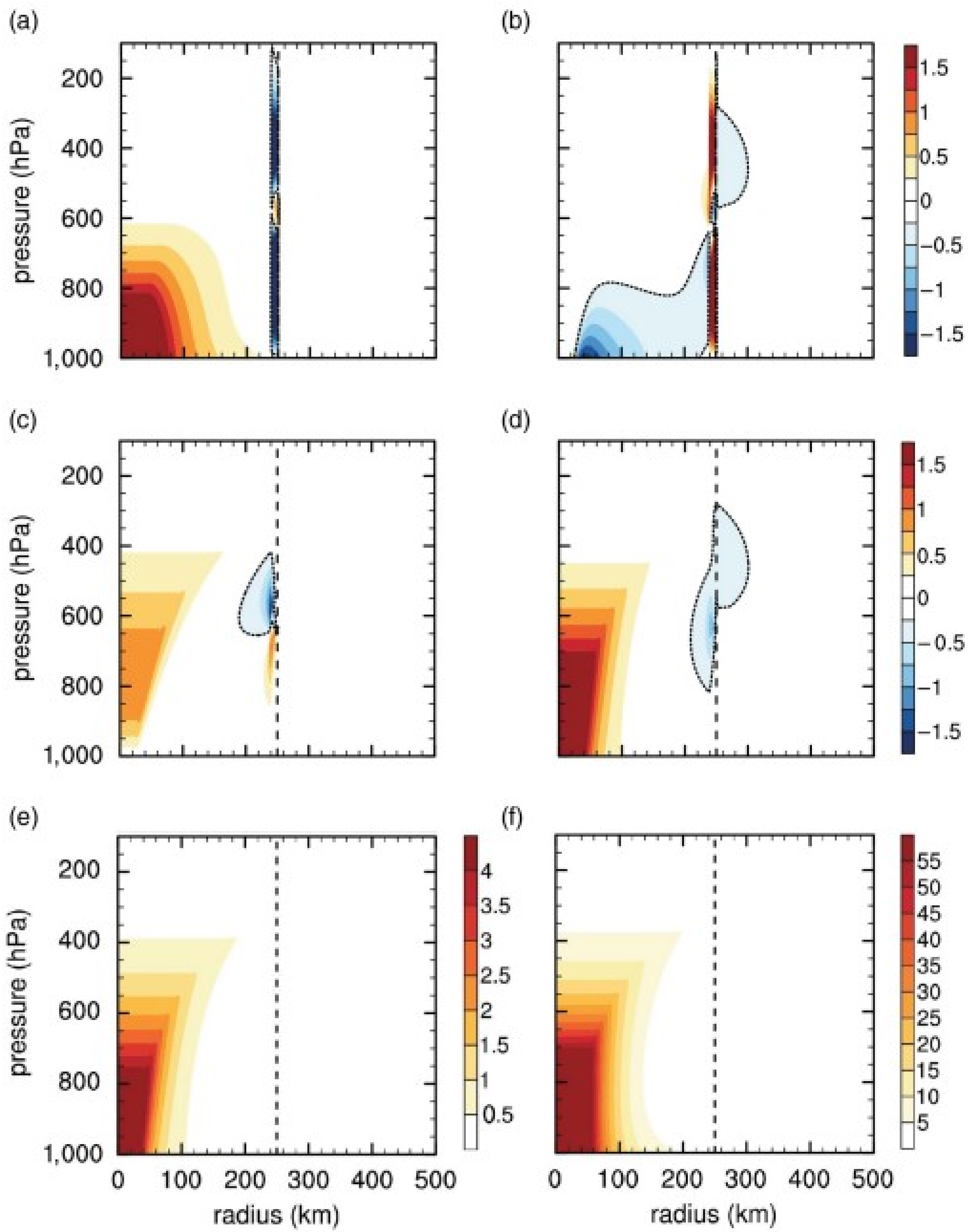

Figure 11. As Figure 10, but in response to deep convective heating

For the response to the combined heating (stratiform plus deep convective), the stretching-like diabatic PV tendency extends through the middle and lower troposphere but peaks near the surface (Figure 12), resembling the vertical diabatic tendency in YOTC data. Horizontal convergence between

1,000 and 500 hPa advects lower-PV air into the heated region, while vertical advection opposes the diabatic tendencies. The total PV tendency peaks near 550 hPa. Unlike the response to isolated stratiform and deep convective heatings, PV and absolute vorticity have disparate vertical structures here, with PV peaking near 550 hPa and absolute vorticity peaking at the surface. The axisymmetric model captures most of the key characteristics of PV evolution in the YOTC composite, namely the bottom-heavy diabatic PV tendency, radial advection of environmental PV by the horizontally convergent flow, growth of mid-level PV and bottom-heavy absolute vorticity, and the smaller radial extent of PV compared to the heating.

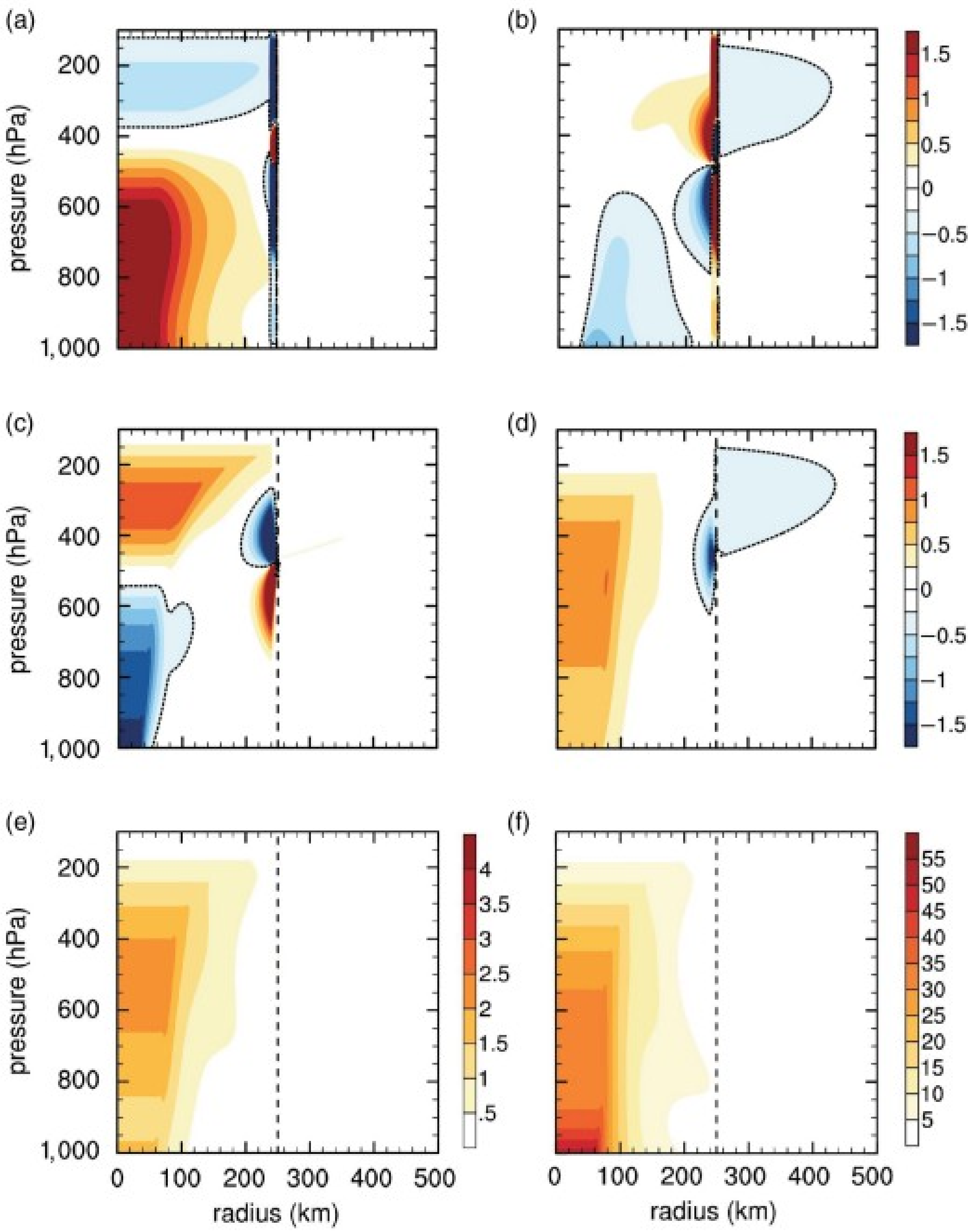

Figure 12. As Figure 10, but in response to a combination of stratiform and deep convective heating

Nonlinear interactions lead to the formation of the mid-level vortex, as evidenced by comparing the response to the combined heating with the sum of the individual responses to stratiform and deep convective heating (Figure 13). While vertical advection produces strong negative tendencies in the lower troposphere in response to the combined heating (Figure 12c), vertical advective tendencies are positive at all levels in the individual responses to isolated deep convective and stratiform heatings (Figures 10c and 11c). Hence, the sum of the individual responses results in bottom-heavy PV and absolute vorticity distributions (Figure 13e,f) distinct from the combined response and the YOTC profiles. This makes sense when one considers the vertical structures of ω and diabatic PV generation induced by deep convective and stratiform heatings; ω induced by deep convective heating will produce a negative advective tendency in the lower troposphere when it acts on the PV diabatically generated by the stratiform heating. A negative advective tendency will also be produced in the lower troposphere when stratiform vertical motion acts on the PV diabatically generated by the deep convective heating. Thus, the interaction of stratiform and deep convective modes is crucial for simultaneous formation of the mid-level PV maximum and low-level absolute vorticity maximum.

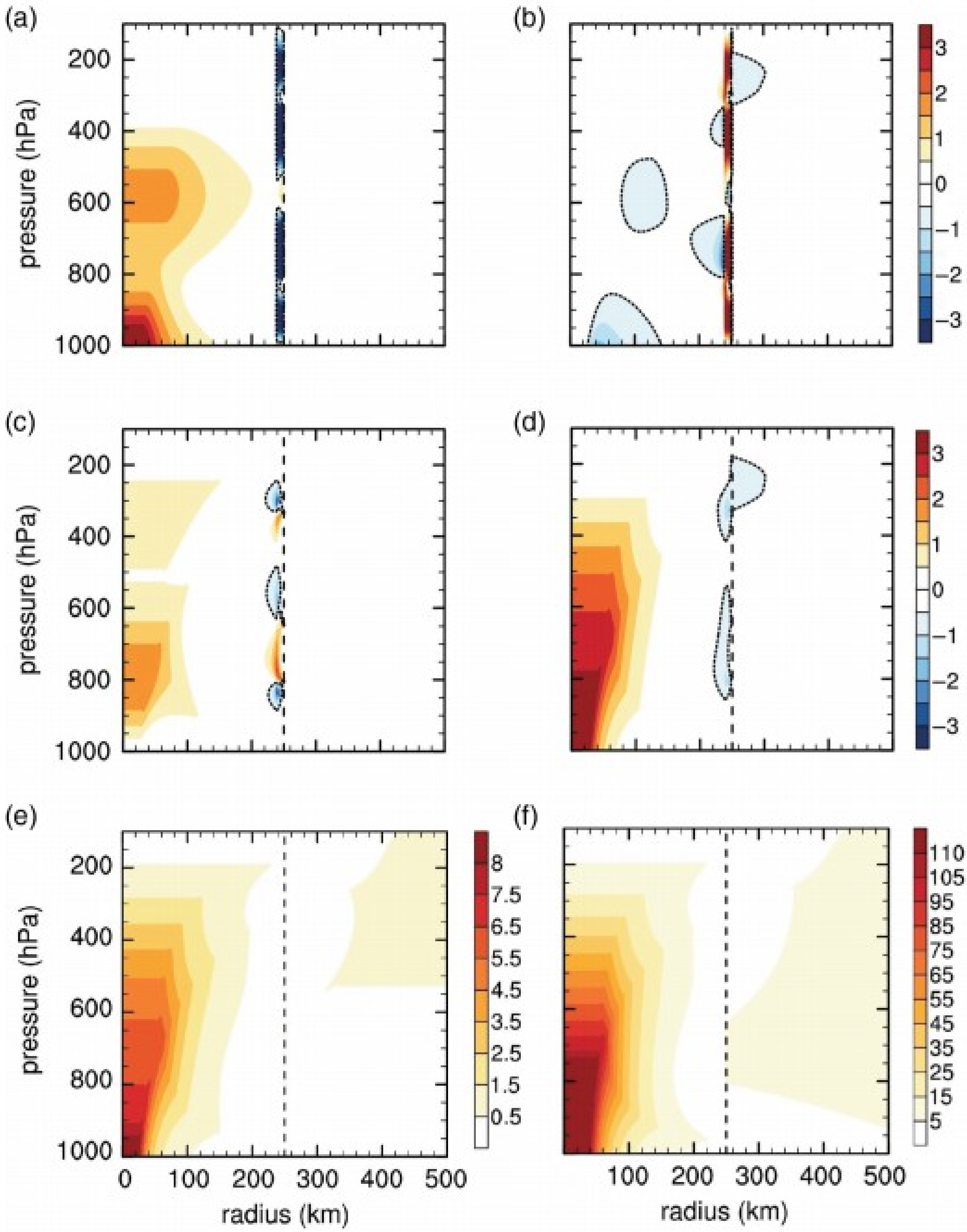

Figure 13. As Figure 10, but for the linear combination of the responses to stratiform and deep convective heating. Note the change in colour scale compared to Figure 10

The PV evolution is well summarized by horizontal averages of tendencies within the heated region (Figure 14). In response to stratiform heating, the combined effects of diabatic and adiabatic tendencies is a mid-level PV maximum near 550 hPa, whereas deep convective heating generates a near-surface PV maximum. When a combination of stratiform and deep convective heating is used, diabatic PV generation is bottom-heavy, but together with adiabatic advection it creates a mid-level PV maximum and bottom-heavy absolute vorticity.

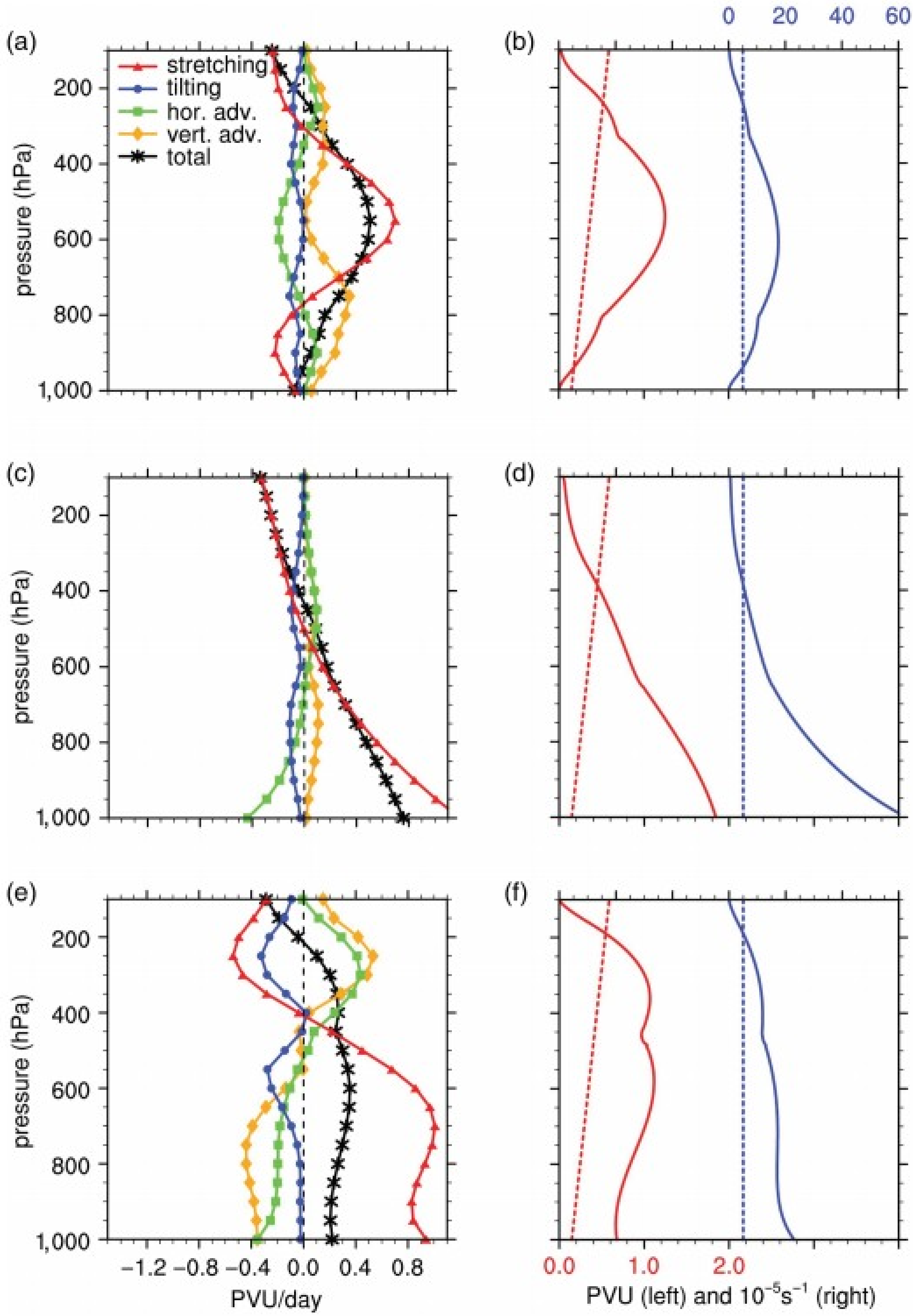

Figure 14. As Figure 9, but in the 2D axisymmetric model. Vertical profiles are obtained by computing radial averages within the heated region ($r < R_O$)

6 SUMMARY AND DISCUSSION

In the composite mean, Atlantic TDs have a mid-level PV maximum near 550 hPa, a substantially higher altitude than that of maxima in absolute vorticity or isentropic PVS. The coincidence of the PV maximum with the melting level suggested the possibility that the PV maximum is diabatically generated by stratiform convection, but the role of adiabatic advection and deep convective heating in shaping the PV structure had remained unclear. Indeed, both YOTC and TRMM estimates revealed a total diabatic PV tendency resembling the bottom-heavy structure expected from deep convective heating. Adiabatic advective tendencies estimated from YOTC were strongly negative in the lower troposphere and thus of the correct qualitative structure to produce a mid-level PV maximum, but large budget residuals prevented a clear conclusion based on that reanalysis product.

In constructing an idealized model to better understand the evolution of PV and absolute vorticity during TD spin-up, we employed the WTG approximation for conceptual simplicity. Under WTG, the conservation equations for isobaric PV, isobaric absolute vorticity, and isentropic PVS all become isomorphic; using the elegant and simple flux form of these equations then becomes attractive, especially because the diabatic tendencies vanish when integrated over the region where $\dot{\theta} > 0$. However, construction of a 1D model from the integrated flux form equations requires knowledge of the radial structure of PV, greatly reducing the utility of such a model. Assuming radially uniform PV may be accurate in regions of horizontal divergence (e.g. Sobel *et al*. 2001), but the radial scale of a cyclonic PV anomaly is greatly reduced by the concentration of PVS in horizontally convergent flow (e.g. Haynes and McIntyre, 1987).

Our 2D axisymmetric model proved more useful, showing that stratiform heating is indeed necessary to generate a mid-level PV maximum, but deep convective heating is needed to simultaneously generate a bottom-heavy profile of absolute vorticity similar to that in observed TDs. Interactions between the deep convective and stratiform modes, which could be called nonlinear, are crucial for transforming the bottom-heavy total diabatic PV tendencies into a mid-level PV maximum. Specifically, ascent in the deep convective mode produces a negative PV tendency at low levels by vertically advecting PV that is diabatically generated by stratiform heating. Similarly, stratiform vertical motion also produces a negative PV tendency at low levels by vertically advecting PV diabatically generated by deep convective heating. These results are consistent with previous studies showing that both stratiform and deep convective clouds play important roles during TC genesis; in our model they generate a mid-level PV maximum by partially cancelling the bottom-heavy diabatic PV generation. Radial advection also produces important negative PV tendencies in the lower troposphere.

Understanding the processes that create a mid-level PV maximum is important because the vertical structure of PV has implications for vortex motion and intensification. The motion of tropical cyclonic vortices is influenced by beta drift and horizontal advection by the steering flow; given the conserved and invertible nature of PV, the horizontal winds at the altitude of the PV maximum make a large contribution to the steering flow. As discussed in previous work, inspection of the vorticity budget at vertical levels far from those of the PV maximum can yield large cancelling terms, especially in strong vertical wind shear (Hoskins *et al*. 1985; Boos *et al*. 2015). Furthermore, the distribution of ascent and, perhaps, convective heating can be inferred from the PV structure, as demonstrated by Sanders (1984), Raymond and Jiang (1990) and others, providing a closure for problems of hydrodynamic instability (e.g. discussions of moist baroclinic instability in Moorthi and Arakawa, 1985; Cohen and Boos, 2016).

This study has numerous caveats and leaves many open questions. We did not consider the possible influences of vertical wind shear and upper-level disturbances, which could advect PV into the TD, alter ascent, or modify diabatic processes. We focused on the system-scale properties of PV, and did not consider scale interactions with individual convective and stratiform clouds or deviations from axisymmetry such as vortex Rossby waves. Alternate forms of PV developed for moist, convecting atmospheres might also be useful (e.g. Schubert *et al*. 2001; Peng *et al*. 2013). Perhaps most importantly, a complete theory would consider two-way interactions between diabatic heating and PV. Despite these caveats, more clearly understanding the one-way influence on PV of diabatic heating and its associated vertical and radial motions is a step toward such a complete theory.

ACKNOWLEDGEMENTS

This work was supported by Office of Naval Research award N00014-15-1-2531, by the U.S. Department of Energy, Office of Science, Office of Biological and Environmental Research under award number DE-SC0019367, and by the Yale Center for Research Computing. ECMWF-YOTC data were accessed from the ECMWF Data Server, Reading, UK (http://apps.ecmwf.int/datasets/data/yotc-od/). The best track data, IBTrACS, were accessed from the World Data Center for Meteorology, Asheville, NC, USA (https://www.ncdc.noaa.gov/ibtracs/). The TRMM 3G25 gridded latent heating product was accessed from the NASA Goddard Earth Sciences Data and Information Services Center, Greenbelt, MD, USA (https://disc.gsfc.nasa.gov/datasets/). All were accessed 30 March 2019. We thank Brian Tang and an anonymous reviewer whose comments helped improve the manuscript.

REFERENCES

Bell, M.M. and Montgomery, M.T. (2008) Observed structure, evolution, and potential intensity of category 5 hurricane Isabel (2003) from 12 to 14 September. *Monthly Weather Review*, 136(6), 2023– 2046. https://doi.org/10.1175/2007mwr1858.1

Berry, G.J., Reeder, M.J. and Jakob, C. (2012) Coherent synoptic disturbances in the Australian monsoon. *Journal of Climate*, 25(24), 8409– 8421. https://doi.org/10.1175/jcli-d-12-00143.1

Bister, M. and Emanuel, K.A. (1997) The genesis of hurricane *Guillermo*: TEXMEX analyses and a modeling study. *Monthly Weather Review*, 125(10), 2662– 2682. https://doi.org/10.1175/1520-0493(1997)125<2662:tgohgt>2.0.co;2

Boos, W.R., Hurley, J.V. and Murthy, V.S. (2015) Adiabatic westward drift of Indian monsoon depressions. *Quarterly Journal of the Royal Meteorological Society*, 141, 1035– 1048. https://doi.org/10.1002/qj.2454

Boos, W.R., Mapes, B.E. and Murthy, V.S. (2017). Potential vorticity structure and propagation mechanism of Indian monsoon depressions, Chapter 15 in The Global Monsoon System, pp. 187– 199, DOI 10.1142/10305, (to appear in print). Chih-Pei Chang, C-P, Kuo, H-C, Lau, N-C, Johnson, RH, Wang, B, Wheeler, MC (eds). World Scientific, Singapore.

Bosart, L.F. and Bartlo, J.A. (1991) Tropical storm formation in a baroclinic environment. *Monthly Weather Review*, 119(8), 1979– 2013. https://doi.org/10.1175/1520-0493(1991)119<1979:tsfiab>2.0.co;2

Cecelski, S.F. and Zhang, D.L. (2016) Genesis of hurricane *Julia* (2010) within an African easterly wave: sensitivity to ice microphysics. *Journal of Applied Meteorology and Climatology*, 55(1), 79– 92. https://doi.org/10.1175/jamc-d-15-0105.1

Chan, J.C. (2005) The physics of tropical cyclone motion. *Annual Review of Fluid Mechanics*, 37(1), 99– 128. https://doi.org/10.1146/annurev.fluid.37.061903.175702

Chan, J.C.L., Ko, F.M.F. and Lei, Y.M. (2002) Relationship between potential vorticity tendency and tropical cyclone motion. *Journal of the Atmospheric Sciences*, 59(8), 1317– 1336. https://doi.org/10.1175/1520-0469(2002)059<1317:rbpvta>2.0.co;2

Cohen, N.Y. and Boos, W.R. (2016) Perspectives on moist baroclinic instability: implications for the growth of monsoon depressions. *Journal of the Atmospheric Sciences*, 73(4), 1767– 1788. https://doi.org/10.1175/jas-d-15-0254.1

de Vries, H., Methven, J., Frame, T.H.A. and Hoskins, B.J. (2010) Baroclinic waves with parameterized effects of moisture interpreted using Rossby wave components. *Journal of the Atmospheric Sciences*, 67(9), 2766– 2784. https://doi.org/10.1175/2010jas3410.1

Dee, D.P., Uppala, S.M., Simmons, A.J., Berrisford, P., Poli, P., Kobayashi, S., Andrae, U., Balmaseda, M.A., Balsamo, G., Bauer, P., Bechtold, P., Beljaars, A.C.M., van de Berg, L., Bidlot, J., Bormann, N., Delsol, C., Dragani, R., Fuentes, M., Geer, A.J., Haimberger, L., Healy, S.B., Hersbach, H., Hólm, E.V., Isaksen, L., Kållberg, P., Köhler, M., Matricardi, M., McNally, A.P., Monge-Sanz, B.M., Morcrette, J.-J., Park, B.K., Peubey, C., de Rosnay, P., Tavolato, C., Thépaut, J.-N. and Vitart, F. (2011) The ERA-interim reanalysis: configuration and performance of the data assimilation system. *Quarterly Journal of the Royal Meteorological Society*, 137, 553– 597. https://doi.org/10.1002/qj.828

Delden, A.V. (2003) Adjustment to heating, potential vorticity and cyclogenesis. *Quarterly Journal of the Royal Meteorological Society*, 129, 3305– 3322. https://doi.org/10.1256/qj.01.65

Ditchek, S.D., Boos, W.R., Camargo, S.J. and Tippett, M.K. (2016) A genesis index for monsoon disturbances. *Journal of Climate*, 29(14), 5189– 5203. https://doi.org/10.1175/jcli-d-15-0704.1

Eliassen, A. (1951) Slow thermally or frictionally controlled meridional circulation in a circular vortex. *Astrophysica Norvegica*, 5, 19

Emanuel, K.A. (2003) Tropical cyclones. *Annual Review of Earth and Planetary Sciences*, 31(1), 75– 104. https://doi.org/10.1146/annurev.earth.31.100901.141259

Ertel, H. (1942) Ein neuer hydrodynamischer Wirbelsatz. *Meteorologische Zeitschrift*, 59, 277– 281

Fritz, C., Wang, Z., Nesbitt, S.W. and Dunkerton, T.J. (2016) Vertical structure and contribution of different types of precipitation during Atlantic tropical cyclone formation as revealed by TRMM PR. *Geophysical Research Letters*, 43(2), 894– 901. https://doi.org/10.1002/2015gl067122

Hack, J.J. and Schubert, W.H. (1986) Nonlinear response of atmospheric vortices to heating by organized cumulus convection. *Journal of the Atmospheric Sciences*, 43(15), 1559– 1573. https://doi.org/10.1175/1520-0469(1986)043<1559:nroavt>2.0.co;2

Hausman, S.A., Ooyama, K.V. and Schubert, W.H. (2006) Potential vorticity structure of simulated hurricanes. *Journal of the Atmospheric Sciences*, 63(1), 87– 108. https://doi.org/10.1175/jas3601.1

Haynes, P.H. and McIntyre, M.E. (1987) On the evolution of vorticity and potential vorticity in the presence of diabatic heating and frictional or other forces. *Journal of the Atmospheric Sciences*, 44(5), 828– 841. https://doi.org/10.1175/1520-0469(1987)044<0828:oteova>2.0.co;2

Haynes, P.H. and McIntyre, M.E. (1990) On the conservation and impermeability theorems for potential vorticity. *Journal of the Atmospheric Sciences*, 47(16), 2021– 2031. https://doi.org/10.1175/1520-0469(1990)047<2021:otcait>2.0.co;2

Hendricks, E.A., Montgomery, M.T. and Davis, C.A. (2004) The role of “vortical” hot towers in the formation of tropical cyclone *Diana* (1984). *Journal of the Atmospheric Sciences*, 61(11), 1209– 1232. https://doi.org/10.1175/1520-0469(2004)061<1209:trovht>2.0.co;2

Hoskins, B.J., McIntyre, M.E. and Robertson, A.W. (1985) On the use and significance of isentropic potential vorticity maps. *Quarterly Journal of the Royal Meteorological Society*, 111, 877– 946. https://doi.org/10.1256/smsqj.47001

Houze, R.A. (1982) Cloud clusters and large-scale vertical motions in the tropics. *Journal of the Meteorological Society of Japan. Series II*, 60(1), 396– 410. https://doi.org/10.2151/jmsj1965.60.1_396

Houze, R.A. (1989) Observed structure of mesoscale convective systems and implications for large-scale heating. *Quarterly Journal of the Royal Meteorological Society*, 115, 425– 461. https://doi.org/10.1002/qj.49711548702

Houze, R.A. (1997) Stratiform precipitation in regions of convection: a meteorological paradox?. *Bulletin of the American Meteorological Society*, 78(10), 2179– 2196. https://doi.org/10.1175/1520-0477(1997)078<2179:spiroc>2.0.co;2

Houze, R.A. (2014) Nimbostratus and the separation of convective and stratiform precipitation. *International Geophysics*, 141– 163. https://doi.org/10.1016/b978-0-12-374266-7.00006-8

Houze, R.A., Lee, W.C. and Bell, M.M. (2009) Convective contribution to the genesis of hurricane *Ophelia* (2005). *Monthly Weather Review*, 137(9), 2778– 2800. https://doi.org/10.1175/2009mwr2727.1

Hunt, K.M.R., Turner, A.G., Inness, P.M., Parker, D.E. and Levine, R.C. (2016) On the structure and dynamics of Indian monsoon depressions. *Monthly Weather Review*, 144(9), 3391– 3416. https://doi.org/10.1175/mwr-d-15-0138.1

Hurley, J.V. and Boos, W.R. (2015) A global climatology of monsoon low-pressure systems. *Quarterly Journal of the Royal Meteorological Society*, 141, 1049– 1064. https://doi.org/10.1002/qj.2447

Kepert, J.D. (2010). Tropical cyclone structure and dynamics, In Global Perspectives on Tropical Cyclones, pp. 3– 53, DOI 10.1142/9789814293488_0001, (to appear in print). Chan, JCL, Kepert, JD (eds), World Scientific, Singapore.

Khairoutdinov, M. and Emanuel, K. (2013) Rotating radiative-convective equilibrium simulated by a cloud-resolving model. *Journal of Advances in Modeling Earth Systems*, 5(4), 816– 825. https://doi.org/10.1002/2013ms000253

Kilroy, G., Smith, R.K. and Montgomery, M.T. (2018) The role of heating and cooling associated with ice processes on tropical cyclogenesis and intensification. *Quarterly Journal of the Royal Meteorological Society*, 144, 99– 114. https://doi.org/10.1002/qj.3187

Knapp, K.R., Kruk, M.C., Levinson, D.H., Diamond, H.J. and Neumann, C.J. (2010) The international best track archive for climate stewardship (IBTrACS). *Bulletin of the American Meteorological Society*, 91(3), 363– 376. https://doi.org/10.1175/2009bams2755.1

Lussier, L.L., Montgomery, M.T. and Bell, M.M. (2014) The genesis of typhoon *Nuri* as observed during the tropical cyclone structure 2008 (TCS-08) field experiment – part 3: dynamics of low-level spin-up during the genesis. *Atmospheric Chemistry and Physics*, 14(16), 8795– 8812. https://doi.org/10.5194/acp-14-8795-2014

McIntyre, M.E. (1993). Isentropic distributions of potential vorticity and their relevance to tropical cyclone dynamics, in Proc. ICSU/WMO International Symposium on Tropical Cyclone Disasters, pp. 143– 156. Beijing University Press, Beijing. Lighthill, MJ, Zheng, Z, Holland, G, Emanuel, KA (eds).

Molinari, J., Skubis, S., Vollaro, D., Alsheimer, F. and Willoughby, H.E. (1998) Potential vorticity analysis of tropical cyclone intensification. *Journal of the Atmospheric Sciences*, 55(16), 2632– 2644. https://doi.org/10.1175/1520-0469(1998)055<2632:pvaotc>2.0.co;2

Möller, J.D. and Smith, R.K. (1994) The development of potential vorticity in a hurricane-like vortex. *Quarterly Journal of the Royal Meteorological Society*, 120, 1255– 1265. https://doi.org/10.1002/qj.49712051907

Moncrieff, M.W., Waliser, D.E., Miller, M.J., Shapiro, M.A., Asrar, G.R. and Caughey, J. (2012) Multiscale convective organization and the YOTC virtual global field campaign. *Bulletin of the American Meteorological Society*, 93(8), 1171– 1187. https://doi.org/10.1175/bams-d-11-00233.1

Montgomery, M.T. and Smith, R.K. (2017) Recent developments in the fluid dynamics of tropical cyclones. *Annual Review of Fluid Mechanics*, 49(1), 541– 574. https://doi.org/10.1146/annurev-fluid-010816-060022

Moorthi, S. and Arakawa, A. (1985) Baroclinic instability with cumulus heating. *Journal of the Atmospheric Sciences*, 42(19), 2007– 2031. https://doi.org/10.1175/1520-0469(1985)042<2007:biwch>2.0.co;2

Muller, C.J. and Romps, D.M. (2018) Acceleration of tropical cyclogenesis by self-aggregation feedbacks. *Proceedings of the National Academy of Sciences*, 115(12), 2930– 2935. https://doi.org/10.1073/pnas.1719967115

Murthy, V.S. and Boos, W.R. (2018) Role of surface enthalpy fluxes in idealized simulations of tropical depression spinup. *Journal of the Atmospheric Sciences*, 75, 1811– 1831. https://doi.org/10.1175/jas-d-17-0119.1

Nolan, D.S. (2007) What is the trigger for tropical cyclogenesis?. *Australian Meteorological Magazine*, 56(4), 241– 266

Peng, J., Zhang, L., Zhang, Y. and Zhu, J. (2013) A modified moist potential vorticity, its properties, and application. *Journal of Geophysical Research:*

Atmospheres, 118(23), 12999– 13007. https://doi.org/10.1002/2013jd020204

Raymond, D., Fuchs, Ž., Gjorgjievska, S. and Sessions, S. (2015) Balanced dynamics and convection in the tropical troposphere. *Journal of Advances in Modeling Earth Systems*, 7(3), 1093– 1116. https://doi.org/10.1002/2015ms000467

Raymond, D.J. (1992) Nonlinear balance and potential vorticity thinking at large Rossby number. *Quarterly Journal of the Royal Meteorological Society*, 118, 987– 1015. https://doi.org/10.1002/qj.49711850708

Raymond, D.J. (2012) Balanced thermal structure of an intensifying tropical cyclone. *Tellus A*, 64(1). https://doi.org/10.3402/tellusa.v64i0.19181

Raymond, D.J. and Jiang, H. (1990) A theory for long-lived mesoscale convective systems. *Journal of the Atmospheric Sciences*, 47(24), 3067–3077. https://doi.org/10.1175/1520-0469(1990)047<3067:atfllm>2.0.co;2

Raymond, D.J., López-Carrillo, C. and Cavazos, L.L. (1998) Case-studies of developing East Pacific easterly waves. *Quarterly Journal of the Royal Meteorological Society*, 124, 2005– 2034. https://doi.org/10.1256/smsqj.55010

Raymond, D.J. and Sessions, S.L. (2007) Evolution of convection during tropical cyclogenesis. *Geophysical Research Letters*, 34(6). https://doi.org/10.1029/2006gl028607

Ritchie, E.A. and Holland, G.J. (1997) Scale interactions during the formation of typhoon *Irving*. *Monthly Weather Review*, 125(7), 1377– 1396. https://doi.org/10.1175/1520-0493(1997)125<1377:sidtfo>2.0.co;2

Rogers, R. (2010) Convective-scale structure and evolution during a high-resolution simulation of tropical cyclone rapid intensification. *Journal of the Atmospheric Sciences*, 67(1), 44– 70. https://doi.org/10.1175/2009jas3122.1

Rossby, C.-G. (1940) Planetary flow patterns in the atmosphere. *Quarterly Journal of the Royal Meteorological Society*, 66, 68– 87

Sanders, F. (1984) Quasi-geostrophic diagnosis of the monsoon depression of 5–8 July 1979. *Journal of the Atmospheric Sciences*, 41(4), 538– 552. https://doi.org/10.1175/1520-0469(1984)041<0538:qgdotm>2.0.co;2

Schenkel, B.A. and Hart, R.E. (2012) An examination of tropical cyclone position, intensity, and intensity life cycle within atmospheric reanalysis datasets. *Journal of Climate*, 25(10), 3453– 3475. https://doi.org/10.1175/2011jcli4208.1

Schubert, W.H. and Alworth, B.T. (1987) Evolution of potential vorticity in tropical cyclones. *Quarterly Journal of the Royal Meteorological Society*, 113, 147– 162. https://doi.org/10.1256/smsqj.47508

Schubert, W.H., Hausman, S.A., Garcia, M., Ooyama, K.V. and Kuo, H.C. (2001) Potential vorticity in a moist atmosphere. *Journal of the Atmospheric Sciences*, 58(21), 3148– 3157. https://doi.org/10.1175/1520-0469(2001)058<3148:pviama>2.0.co;2

Seager, R. and Henderson, N. (2013) Diagnostic computation of moisture budgets in the ERA-Interim reanalysis with reference to analysis of CMIP-archived atmospheric model data. *Journal of Climate*, 26(20), 7876– 7901. https://doi.org/10.1175/jcli-d-13-00018.1

Shapiro, L.J. (1996) The motion of hurricane *Gloria*: a potential vorticity diagnosis. *Monthly Weather Review*, 124(11), 2497– 2508. https://doi.org/10.1175/1520-0493(1996)124<2497:tmohga>2.0.co;2

Shapiro, L.J. and Franklin, J.L. (1995) Potential vorticity in hurricane *Gloria*. *Monthly Weather Review*, 123(5), 1465– 1475. https://doi.org/10.1175/1520-0493(1995)123<1465:pvihg>2.0.co;2

Shige, S., Takayabu, Y.N., Tao, W.K. and Johnson, D.E. (2004) Spectral retrieval of latent heating profiles from TRMM PR data. Part I: development of a model-based algorithm. *Journal of Applied Meteorology*, 43(8), 1095– 1113. https://doi.org/10.1175/1520-0450(2004)043<1095:srolhp>2.0.co;2

Shige, S., Takayabu, Y.N., Tao, W.K. and Shie, C.L. (2007) Spectral retrieval of latent heating profiles from TRMM PR data. Part II: algorithm improvement and heating estimates over tropical ocean regions. *Journal of Applied Meteorology and Climatology*, 46(7), 1098– 1124. https://doi.org/10.1175/jam2510.1

Shige, S., Takayabu, Y.N., Kida, S., Tao, W.K., Zeng, X., Yokoyama, C. and L'Ecuyer, T. (2009) Spectral retrieval of latent heating profiles from TRMM PR data. Part IV: comparisons of look-up tables from two- and three-dimensional cloud-resolving model simulations. *Journal of Climate*, 22(20), 5577– 5594. https://doi.org/10.1175/2009jcli2919.1

Smith, R.K. and Montgomery, M.T. (2012) Observations of the convective environment in developing and non-developing tropical disturbances. *Quarterly Journal of the Royal Meteorological Society*, 138, 1721– 1739. https://doi.org/10.1002/qj.1910

Sobel, A.H. and Bretherton, C.S. (2000) Modeling tropical precipitation in a single column. *Journal of Climate*, 13(24), 4378– 4392. https://doi.org/10.1175/1520-0442(2000)013<4378:mtpias>2.0.co;2

Sobel, A.H., Nilsson, J. and Polvani, L.M. (2001) The weak temperature gradient approximation and balanced tropical moisture waves. *Journal of the Atmospheric Sciences*, 58(23), 3650– 3665. https://doi.org/10.1175/1520-0469(2001)058<3650:twtgaa>2.0.co;2

Stoelinga, M.T. (1996) A potential vorticity-based study of the role of diabatic heating and friction in a numerically simulated baroclinic cyclone. *Monthly*

Weather Review, 124(5), 849– 874. https://doi.org/10.1175/1520-0493(1996)124<0849:apvbso>2.0.co;2

Tao, C., Jiang, H. and Zawislak, J. (2017) The relative importance of stratiform and convective rainfall in rapidly intensifying tropical cyclones. *Monthly Weather Review*, 145(3), 795– 809. https://doi.org/10.1175/mwr-d-16-0316.1

Tao, W.K., Smith, E.A., Adler, R.F., Haddad, Z.S., Hou, A.Y., Iguchi, T., Kakar, R., Krishnamurti, T.N., Kummerow, C.D., Lang, S., Meneghini, R., Nakamura, K., Nakazawa, T., Okamoto, K., Olson, W.S., Satoh, S., Shige, S., Simpson, J., Takayabu, Y., Tripoli, G.J. and Yang, S. (2006) Retrieval of latent heating from TRMM measurements. *Bulletin of the American Meteorological Society*, 87(11), 1555– 1572. https://doi.org/10.1175/bams-87-11-1555

Thorpe, A.J. (1985) Diagnosis of balanced vortex structure using potential vorticity. *Journal of the Atmospheric Sciences*, 42(4), 397– 406. https://doi.org/10.1175/1520-0469(1985)042<0397:dobvsu>2.0.co;2

Tory, K.J., Montgomery, M.T., Davidson, N.E. and Kepert, J.D. (2006) Prediction and diagnosis of tropical cyclone formation in an NWP system. Part II: a diagnosis of tropical cyclone *Chris* formation. *Journal of the Atmospheric Sciences*, 63(12), 3091– 3113. https://doi.org/10.1175/jas3765.1

Tory, K.J., Kepert, J.D., Sippel, J.A. and Nguyen, C.M. (2012) On the use of potential vorticity tendency equations for diagnosing atmospheric dynamics in numerical models. *Journal of the Atmospheric Sciences*, 69(3), 942– 960. https://doi.org/10.1175/jas-d-10-05005.1

Wang, Y. (2008) Structure and formation of an annular hurricane simulated in a fully compressible, nonhydrostatic model – TCM4. *Journal of the Atmospheric Sciences*, 65(5), 1505– 1527. https://doi.org/10.1175/2007jas2528.1

Wang, Z. (2012) Thermodynamic aspects of tropical cyclone formation. *Journal of the Atmospheric Sciences*, 69(8), 2433– 2451. https://doi.org/10.1175/jas-d-11-0298.1

Wang, Z. (2014) Role of cumulus congestus in tropical cyclone formation in a high-resolution numerical model simulation. *Journal of the Atmospheric Sciences*, 71(5), 1681– 1700. https://doi.org/10.1175/jas-d-13-0257.1

Wang, Z., Montgomery, M.T. and Dunkerton, T.J. (2010) Genesis of pre-hurricane *Felix* (2007). Part II: warm core formation, precipitation evolution, and predictability. *Journal of the Atmospheric Sciences*, 67(6), 1730– 1744. https://doi.org/10.1175/2010jas3435.1

Wing, A.A., Camargo, S.J. and Sobel, A.H. (2016) Role of radiative–convective feedbacks in spontaneous tropical cyclogenesis in idealized numerical simulations. *Journal of the Atmospheric Sciences*, 73(7), 2633– 2642. https://doi.org/10.1175/jas-d-15-0380.1

Wu, C.C. and Kurihara, Y. (1996) A numerical study of the feedback mechanisms of hurricane–environment interaction on hurricane movement from the potential vorticity perspective. *Journal of the Atmospheric Sciences*, 53(15), 2264– 2282. https://doi.org/10.1175/1520-0469(1996)053<2264:ansotf>2.0.co;2

Yang, Z., Yuan, T., Jiang, H., Zhang, L. and Zhang, C. (2018) Stratiform and convective precipitation properties of tropical cyclones in the Northwest Pacific. *Journal of Geophysical Research: Atmospheres*, 123(7), 3513– 3529. https://doi.org/10.1002/2017jd027174

Yau, M.K., Liu, Y., Zhang, D.L. and Chen, Y. (2004) A multiscale numerical study of hurricane *Andrew* (1992). Part VI: small-scale inner-core structures and wind streaks. *Monthly Weather Review*, 132(6), 1410– 1433. https://doi.org/10.1175/1520-0493(2004)132<1410:amnsoh>2.0.co;2

Yu, Z., Liang, X., Yu, H. and Chan, J.C.L. (2010) Mesoscale vortex generation and merging process: a case study associated with a post-landfall tropical depression. *Advances in Atmospheric Sciences*, 27(2), 356– 370. https://doi.org/10.1007/s00376-009-8091-x

Yuan, J. and Wang, D. (2014) Potential vorticity diagnosis of tropical cyclone *Usagi* (2001) genesis induced by a mid-level vortex over the South China Sea. *Meteorology and Atmospheric Physics*, 125(1-2), 75– 87. https://doi.org/10.1007/s00703-014-0316-6

Zawislak, J. and Zipser, E.J. (2014a) Analysis of the thermodynamic properties of developing and nondeveloping tropical disturbances using a comprehensive dropsonde dataset. *Monthly Weather Review*, 142(3), 1250–1264. https://doi.org/10.1175/mwr-d-13-00253.1

Zawislak, J. and Zipser, E.J. (2014b) A multisatellite investigation of the convective properties of developing and nondeveloping tropical disturbances. *Monthly Weather Review*, 142(12), 4624– 4645. https://doi.org/10.1175/mwr-d-14-00028.1